



# Stress concentration issues in unidirectional laminates

Lucas Lisbôa Vignoli<sup>1</sup> · Jaime Tupiassú Pinho de Castro<sup>2</sup> · Marco Antonio Meggiolaro<sup>2</sup>

Received: 29 March 2019 / Accepted: 9 September 2019 / Published online: 30 September 2019  
© The Brazilian Society of Mechanical Sciences and Engineering 2019

## Abstract

This paper analytically studies how elliptical holes affect the resistance of unidirectional laminate plates. Although local stress and strain concentration effects induced by notches are well known in isotropic materials, the same cannot be said about anisotropic materials. Stroh formalism is used to describe the elastic stresses around the border of elliptical holes subjected to in-plane loads. Tsai–Wu, Puck, and LaRC05 failure criteria are applied to estimate initial damage, due to their good performance on the world-wide failure exercise. Plane strain conditions are also studied to evaluate 3D constraint effects induced by the plate thickness. The major conclusions are: (1) the stress concentration may be up to about twice higher than for isotropic materials; (2) matrix failure is observed for most cases, and the notched strength is smaller than 10% of the unnotched strength; (3) strength prediction differences assuming plane stress and plane strain limit cases may be higher than 50%; and (4) for compressive loads, the LaRC05 model predicts a considerable strength reduction when compared to the other failure criteria.

**Keywords** Composite · Stress concentration · Stroh formalism

## 1 Introduction

Notches like holes, slots, grooves, keyways, shoulders, corners, threads, reinforcements, etc., are usually unavoidable in real structural components for functional or manufacturing reasons, but they introduce local stress/strain concentration effects that cannot be neglected in most practical applications. Such effects are usually analytically modeled considering bi-dimensional (2D) plane stress or plane strain approximations, as exhaustively discussed by Savin [1]. Studies of 3D notch effects in isotropic materials can also be found in the literature too, see, e.g., [2]. For stress analyses in anisotropic materials, Lekhniskii [3] and Stroh

[4] formalisms are popular, and both can be used to generate exact elastic 2D solutions for concentration effects induced by circular and elliptical holes in infinite plates, as well as approximated solutions for other notch shapes [5, 6]. Tan [7, 8] proposed some useful functions to approximately describe stress gradients around elliptical holes, which play an important role in early crack growth [9]. Zappalorto and Carraro [10] proposed an approximated analysis for hyperbolic notches. A brief overview of the general 2D problems in anisotropic materials is presented by Sevenois and Kousios [11]. However, these works use stress concentration factors instead of the complete stress distribution around the notch, following the usual approach for isotropic materials. In Sect. 3, the importance of considering the whole stress distribution for anisotropic materials is discussed.

Strength estimations for notched laminates are not a simple task at all. Analytically, a few models like those proposed by Whitney and Nuismer [12] and by Tan [7, 8] are traditionally used because they can provide a relatively good approximation for some laminates. However, both models need to use adjustable experimental parameters that depend on the laminated material, layout type and other factors, and do not reproduce the physical failure mechanisms.

Recently, this problem has been widely analyzed. Experimentally, Iarve et al. [13] and Mollenhauer et al. [14] used Moiré interferometric techniques to evaluate damage

---

Technical Editor: Paulo de Tarso Rocha de Mendonça, Ph.D.

✉ Lucas Lisbôa Vignoli  
ll.vignoli@mecanica.coppe.ufrj.br

Jaime Tupiassú Pinho de Castro  
jtcastro@puc-rio.br

Marco Antonio Meggiolaro  
meggi@puc-rio.br

<sup>1</sup> Department of Mechanical Engineering, UFRJ - Campus Macaé, Macaé, Brazil

<sup>2</sup> Department of Mechanical Engineering, PUC-Rio, Rio de Janeiro, Brazil

progression and stress redistribution during failure evolution. O'Higgins et al. [15] compared some characteristics of glass fiber and carbon fiber open-hole composites and concluded that the glass fibers allow a higher strain level, whereas the carbon fibers provide stiffer laminates. Lee and Soutis [16] carried out a detailed and comprehensive study about how the specimen dimension affects the measured strength. Huang et al. [17] proposed a new specimen design to get a more uniform stress distribution in biaxial tests. Kureemun et al. [18] tested biaxial open-hole specimens under tension/compression, helping to fill this experimental data gap in the literature. Shah et al. [19] proposed the use of numerical tools (instead of experimental) to estimate the strength of laminates under biaxial loads because of their cost advantage. However, since experimental data depend on many factors, such as hole shape and dimensions, it is necessary to collect a large amount of data from different tests to obtain the data basis necessary for design purposes. Chen et al. [20] and Su et al. [21] analyzed the effect of the finite elements used for fracture simulation under uniaxial tension and compression, and of geometrical parameters like hole dimension and plate thickness. Other simulation approaches, like those proposed by Sadeghi et al. [22] and by Moure et al. [23], study as well the potential for numerical simulations in this field.

However, despite all these investigations, a comprehensive parametric study of notch effects on composite structural components still is not available. Hence, there is room for limit analytical solutions in this field. Indeed, since the design of composite structural components involves a large amount of variables, numerical simulations can become very expensive or even unsuitable for some practical applications, and analytical models can be a very useful tool in such cases [24]. For instance, the importance of parametric analytical analyses for the design of composite pressure vessels is studied in [25].

In the following sections, first the Stroh formalism is used to obtain the solution for the stress distribution around elliptical holes in orthotropic plates under plane stress conditions. A study about other notch types is presented by Zapalorto and Carraro [26, 27]. An alternative solution, valid just for orthotropic materials, is presented by Bonora et al. [28, 29]. However, considering unidirectional laminates, Bonora's approach cannot model off-axis loads.

The stress distribution proposed here can be generalized for any anisotropic material, as well as for plane strain conditions, as proved by Ting [4] and Hwu [6]. It can also be extended, using the classical laminate theory (CLT), to obtain equivalent mechanical properties, which transform a laminate layup in an equivalent uniform homogenized orthotropic plate. The CLT may be useful as first approach to study stress concentration effect in multidirectional symmetric laminates, but numerical simulations must be

carried out to evaluate out-of-plane stresses and strains around the hole due to border effects. The stress distribution around elliptical notches developed here is used to estimate the initial damage of notched plates by three different criteria, using the world-wide failure exercise (WWFE) results as a basis [30], considering both the first (WWFE-I) [31] and the second (WWFE-II) [32] editions recommended guideline. Finally, plane strain conditions are considered to evaluate the possible error generated by neglecting the transversal stress component along the plate thickness direction when plane stress is assumed around the notch border. Even though plane stress and plane strain are simplified limit assumptions to analyze 3D structures as if it was a 2D problem, the actual stress components and strengths for any plate thickness are expected to be between these two bounds.

## 2 Theoretical basis

Four principal coordinate systems are used to study the stress concentration problem in anisotropic plates, as shown in Fig. 1. Global coordinates  $x_i^{(g)}$  are used for the applied load. The material coordinates are  $x_i$ , where  $x_1$  is aligned to the fibers and the angle between  $x_1$  and  $x_1^{(g)}$  is  $\alpha$ . The elliptical hole geometry is defined by  $x_i^{(h)}$ , where the angle between  $x_1^{(h)}$  and  $x_1$  is  $\beta$ . Finally, the elliptical hole border is mapped by the local coordinates  $x_i^{(l)}$ , where the angle between  $x_1^{(l)}$  and  $x_1$  is  $\theta$ . The operator used to rotate tensors from one coordinate system to another can be defined as  $\lambda_{ij} = \cos(x_i, x_j)$  [33].

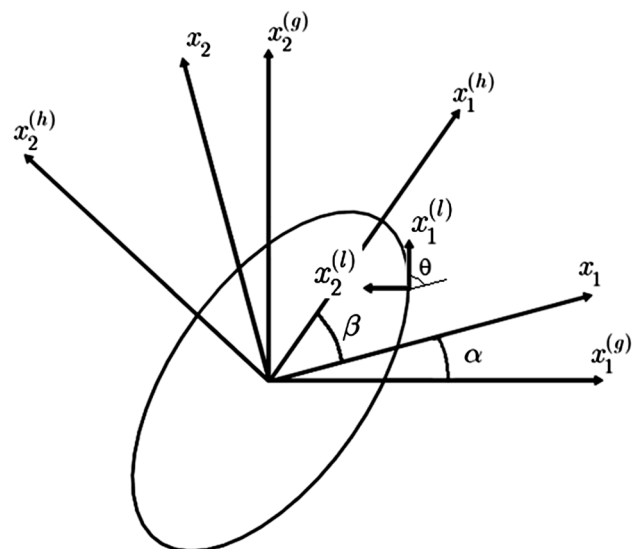


**Fig. 1** Coordinate systems used to model stresses and strains around elliptical hole borders in anisotropic plates

### 2.1 Stroh formalism

The Stroh formalism is a powerful analytical tool to model anisotropic materials, and it is used herein considering general orthotropic materials. An overview of the formalism is presented next, but further detailed derivations can be found in Ting [4] and Hwu [6]. As in all elasticity problems, the equilibrium requirements (neglecting body forces), the geometrical compatibility and the constitutive equations must be satisfied by obeying the following equations:

$$\sigma_{ij,j} = 0 \tag{1}$$

$$\varepsilon_{ij} = (u_{i,j} + u_{j,i})/2 \tag{3}$$

$$\sigma_{ij} = s_{ijkl}\varepsilon_{kl} \tag{3}$$

The general solution for the displacement field  $u_k$  is obtained by

$$u_k = a_k f_k(z_k) \tag{4}$$

The constants  $a_k$  in Eq. (4) depend on material properties, which are defined as the material eigenvectors, and  $f_k(z_k)$  are functions obtained from the boundary conditions. Considering 2D problems, without loss of generality,  $z_k = x_1 + p_k x_2$ , where  $p_k$  are the material eigenvalues computed by manipulating Eqs. (1–4) to obtain

$$[\mathbf{Q} + (\mathbf{R} + \mathbf{R}^T)p + \mathbf{T}p^2]\mathbf{a} = \mathbf{0} \tag{5}$$

where  $Q_{ik} = s_{i1k1}$ ,  $R_{ik} = s_{i1k2}$  and  $T_{ik} = s_{i2k2}$ . Then, the general stress solutions are given by

$$\sigma_{i1} = -pb_j f'(z) \tag{6}$$

$$\sigma_{i2} = b_j f'(z) \tag{7}$$

where  $\mathbf{b} = [\mathbf{R}^T + p\mathbf{T}]\mathbf{a} = -(1/p)[\mathbf{Q} + p\mathbf{R}]\mathbf{a}$ . Using Airy's stress function [31], the general solution for the stress function is

$$\phi_i = b_j f(z) \tag{8}$$

It is helpful to transform Eq. (5) in a classical form of the eigenvalue problem. Using matrix properties and the definition of  $\mathbf{b}$ , the following relation can be obtained

$$\begin{bmatrix} \mathbf{N}_1 & \mathbf{N}_2 \\ \mathbf{N}_3 & \mathbf{N}_1 \end{bmatrix}^T \begin{bmatrix} \mathbf{a} \\ \mathbf{b} \end{bmatrix} = p \begin{bmatrix} \mathbf{a} \\ \mathbf{b} \end{bmatrix} \tag{9}$$

where  $\mathbf{N}_1 = -\mathbf{T}^{-1}\mathbf{R}^T$ ,  $\mathbf{N}_2 = \mathbf{T}^{-1}$  and  $\mathbf{N}_3 = -\mathbf{R}\mathbf{T}^{-1}\mathbf{R}^T - \mathbf{Q}$ .

Considering the local coordinate system, a direct transformation can be obtained by

$$\mathbf{Q}^{(l)} = \mathbf{Q} \cos^2 \theta + (\mathbf{R} + \mathbf{R}^T) \sin \theta \cos \theta + \mathbf{T} \sin^2 \theta \tag{10}$$

$$\mathbf{R}^{(l)} = \mathbf{R} \cos^2 \theta + (\mathbf{T} - \mathbf{Q}) \sin \theta \cos \theta + \mathbf{R}^T \sin^2 \theta \tag{11}$$

$$\mathbf{T}^{(l)} = \mathbf{T} \cos^2 \theta - (\mathbf{R} + \mathbf{R}^T) \sin \theta \cos \theta + \mathbf{Q} \sin^2 \theta \tag{12}$$

Hence,

$$\mathbf{N}_1^{(l)} = -[\mathbf{T}^{(l)}]^{-1} [\mathbf{R}^{(l)}]^T \tag{13}$$

$$\mathbf{N}_2^{(l)} = [\mathbf{T}^{(l)}]^{-1} \tag{14}$$

$$\mathbf{N}_3^{(l)} = -\mathbf{R}^{(l)} [\mathbf{T}^{(l)}]^{-1} [\mathbf{R}^{(l)}]^T - \mathbf{Q}^{(l)} \tag{15}$$

The Barnett–Lothe tensors [34] are defined in the integral form as

$$\mathbf{S}_{BL} = \frac{1}{\pi} \int_0^\pi \mathbf{N}_1^{(l)} d\theta \tag{16}$$

$$\mathbf{H}_{BL} = \frac{1}{\pi} \int_0^\pi \mathbf{N}_2^{(l)} d\theta \tag{17}$$

$$\mathbf{L}_{BL} = \frac{1}{\pi} \int_0^\pi \mathbf{N}_3^{(l)} d\theta \tag{18}$$

Explicit solutions for the Barnett–Lothe tensors can be found in Hwu [6].

The load expressed in global coordinates  $x_i^{(g)}$  can be computed in material coordinates  $x_i$  using

$$\sigma_{ij} = \lambda_{ik} \lambda_{jl} \sigma_{kl}^{(g)} \tag{19}$$

where the angle between  $x_i$  and  $x_i^{(g)}$  is  $\alpha$  (see Fig. 1), and the stress vector can be defined in material coordinates as

$$\tau_i = [\sigma_{i1} \ \sigma_{i2} \ 0]^T, \quad i = 1, 2 \tag{20}$$

Using conformal mapping to transform the ellipse into a unitary circle in complex space, the general form of the stress function that satisfies  $\sigma_{22}^{(l)} = 0$  and yields stress components that tend to the applied load far from the hole is given by

$$\phi = (x_1 \tau_2 - x_2 \tau_1) + 2Re \left\{ \mathbf{B} \left\langle \zeta_\xi^{-1} \right\rangle \mathbf{q} \right\} \tag{21}$$

where  $\zeta$  is used to map the circle on the complex space, the symbol  $\left\langle \zeta_\xi^{-1} \right\rangle$  means a diagonal matrix with the elements  $\zeta_\xi^{-1}$ ,  $\mathbf{B} = [b_1 \ b_2 \ b_3]$ , and  $\mathbf{q}$  is a generic vector to be determined.

The traditional approach [4, 6] fixes the ellipse principal axis, but here it is considered that the ellipse can be inclined in relation to the fiber direction by an angle  $\beta$ , as illustrated in Fig. 1. Then, the elliptical parametric equation is  $x_1 = r_a \cos(\psi + \beta) \cos \beta - r_b \sin(\psi + \beta) \sin \beta$  and

$x_2 = r_a \cos(\psi + \beta) \sin \beta + r_b \sin(\psi + \beta) \cos \beta$ , where  $r_a$  and  $r_b$  are the major and the minor ellipse semi-axes and  $\psi$  is the angle defined on the complex space. Note that when  $\beta = 0^\circ$ , both definitions become identical. Using the free surface boundary condition ( $\sigma_{22}^{(l)} = 0$ ), it is possible to find

$$\mathbf{q} = -(1/2)\mathbf{B}^{-1}[(r_a \cos \beta - ir_b \sin \beta)\boldsymbol{\tau}_2 - (r_a \sin \beta + ir_b \cos \beta)\boldsymbol{\tau}_1] \tag{22}$$

Having obtained the stress function, the stress along the elliptical hole border can be computed as

$$\sigma_{11}^{(l)} = -[\mathbf{e}_1^{(l)}]^T \partial\Phi / \partial\mathbf{e}_2^{(l)} \tag{23}$$

where  $[\mathbf{e}_1^{(l)}]^T = [\cos \theta \ \sin \theta \ 0]$  and  $[\mathbf{e}_2^{(l)}]^T = [-\sin \theta \ \cos \theta \ 0]$  are unit vectors in  $x_1^{(l)}$  and  $x_2^{(l)}$  directions.

The derivative  $\partial\Phi / \partial\mathbf{e}_2^{(l)}$  can be obtained considering an infinitesimal arc of the ellipse  $ds$ , taking care to relate the angles  $\psi$  and  $\theta$  using the infinitesimal triangle of sides  $ds$ ,  $dx_1$  and  $dx_2$ . The result, as a function just of  $\theta$ , is

$$\begin{aligned} \partial\Phi / \partial\mathbf{e}_2^{(l)} = & -\boldsymbol{\tau}_2 \sin \theta - \boldsymbol{\tau}_1 \cos \theta \\ & + \operatorname{Re} \left\{ \left( i \sin(\theta - \beta) - \frac{r_b}{r_a} \cos(\theta - \beta) \right) (\mathbf{G}_1^{(l)} + i\mathbf{G}_3^{(l)}) \left[ \left( \frac{r_a}{r_b} \cos \beta - i \sin \beta \right) \boldsymbol{\tau}_2 - \left( \frac{r_a}{r_b} \sin \beta + i \cos \beta \right) \boldsymbol{\tau}_1 \right] \right\} \end{aligned} \tag{24}$$

where  $\mathbf{G}_1^{(l)} = (\mathbf{N}_1^{(l)})^T - \mathbf{N}_3^{(l)} \mathbf{S}_{BL} (\mathbf{L}_{BL})^{-1}$  and  $\mathbf{G}_3^{(l)} = -\mathbf{N}_3^{(l)} (\mathbf{L}_{BL})^{-1}$ .

Hwu [6] presented an analysis for polygonal and elliptical holes; however, the alternative approach presented above has some practical advantages. Indeed, it uses global coordinates to compute the applied load considering the angle between the ellipse and the material coordinates, so it allows a better view of the hole inclination effect in failure analyses. For a circular hole,  $r_a = r_b = r$ , the hoop stress solution is then given by

$$\sigma_{11}^{(l)} = \mathbf{i}_1 (\mathbf{G}_1^{(l)} \boldsymbol{\tau}_2 + \mathbf{G}_3^{(l)} \boldsymbol{\tau}_1) - \mathbf{i}_2 (\mathbf{G}_1^{(l)} \boldsymbol{\tau}_1 - \mathbf{G}_3^{(l)} \boldsymbol{\tau}_2) \tag{25}$$

where  $\mathbf{i}_1 = [1 \ 0 \ 0]$  and  $\mathbf{i}_2 = [0 \ 1 \ 0]$ .

For some considerations about the classical laminate theory application to extend the Stroh formalism application, see [35–37]. It is well known that interlaminar effects are generated because of the different properties of consecutive laminas in a laminate, see, e.g., Kant and Swaminathan [38], but these effects are not within the scope of this paper.

## 2.2 First-Ply failure analysis

According to Soden et al. [31], Tsai–Wu, Puck, and Cuntze are the anisotropic failure models that better fitted the

WWFE-I data. The latter is not used in this paper because it provides similar predictions to Puck for First-Ply-Failure (FPF) [39]. Kaddour and Hinton [32] say that LaRC05 and Carrere models better described WWFE-II results, but the latter is not considered in this paper either, since it is based on a computational micromechanics approach. So, three failure criteria are used in the following analyses: Tsai–Wu, Puck, and LaRC05.

Tsai–Wu model uses just one polynomial function to fit the data, whereas the others use different functions to separate the concurrent damage mechanisms. A single polynomial equation is easier to implement, but different functions to evaluate different failure mechanisms can be more versatile. Hence, each failure model has advantages and disadvantages, and so far none has been recognized as clearly superior. Indeed, Soden et al. [31] suggest that the safest approach is to use more than one criterion to model composite structures and then to choose the most conservative result to design or analyze them.

A more recent failure design guideline [40] assumes the trace of the stiffness matrix is an invariant for carbon fiber-reinforced polymer (CFRP), so that it can be considered a material property. Hence, this criterion uses omni strain failure envelopes and considers the most conservative one. According to the authors, even using the inner envelope curve, the results allow a strain level higher than usually assumed in industrial practices. However, this new criterion cannot be used here either, because it is not applicable for stress concentration problems, since initial damage estimates using this conservative approach results in a too small strain level on the rest of the structure. Alternatively, even though recent advances in micromechanical modeling may improve its usefulness, macromechanical criteria are selected for the present study, despite limited analysis for specific fiber volume fraction, because they still have a higher reliability than micromechanical models [41].

For all the models presented hereafter, failure is assumed to begin when the function used to describe them equals one. To keep generality, the failure criteria are presented for a 3D stress state.

### 2.2.1 Tsai–Wu criterion

Tsai and Wu proposed a general failure criterion for anisotropic materials [42, 43], not restricted to composites, based

on a polynomial function. Considering a unidirectional composite as transversally isotropic for 3D cases, and considering its different strengths along each direction, this function can be expanded as

$$\begin{aligned}
 f_{TW} = & \frac{\sigma_{11}^2}{S_{11}^t S_{11}^c} + \frac{(\sigma_{22}^2 + \sigma_{33}^2)}{S_{22}^t S_{22}^c} + \frac{\sigma_{12}^2 + \sigma_{13}^2}{(S_{12})^2} + \left(\frac{\sigma_{23}}{S_{23}}\right)^2 \\
 & + a_{12}\sigma_{11}(\sigma_{22} + \sigma_{33}) + a_{23}\sigma_{22}\sigma_{33} + \left(\frac{1}{S_{11}^t} - \frac{1}{S_{11}^c}\right)\sigma_{11} \\
 & + \left(\frac{1}{S_{22}^t} - \frac{1}{S_{22}^c}\right)(\sigma_{22} + \sigma_{33})
 \end{aligned} \tag{26}$$

where  $a_{12}$  and  $a_{23}$  are calibration factors that represent the interaction between normal stresses.

In the absence of experimental data, the following values may be used as a first approximation

$$a_{12} = -\left(\sqrt{S_{11}^t S_{11}^c S_{22}^t S_{22}^c}\right)^{-1} \tag{27}$$

$$a_{23} = -(S_{22}^t S_{22}^c)^{-1} \tag{28}$$

A similar approach based on strains was also proposed, and it can be useful for experimental analyses.

### 2.2.2 Puck criterion

Puck’s theory [44, 45] has been widely used in Germany, inclusive in standard procedures [46], and it became more popular after the WWFE results and the publication of Knops’ book [47]. Using the traditional maximum stress theory as a starting point, the fiber failure criterion under tensile loads can be written as

$$f_P^{(f,t)} = (1/S_{11}^t) \cdot \left| \sigma_{11} + \left[ (E_1/E_1^{(f)}) \nu_{12}^{(f)} m_f - \nu_{12} \right] (\sigma_{22} + \sigma_{33}) \right| \tag{29}$$

where  $m_f$  is a constant used to quantify the effect of different Poisson’s ratios for the fiber and the matrix, which in the absence of experimental data may be considered equal to 1.1 for glass fibers and to 1.3 for carbon fibers embed in polymeric matrices.

As experimentally proved by Puck and Schürmann in [44], shear stresses affect fiber failure under compressive loads, and in this case, the failure function can be expressed as

$$\begin{aligned}
 f_P^{(f,c)} = & (1/S_{11}^c) \left| \sigma_{11} + \left[ (E_1/E_1^{(f)}) \nu_{12}^{(f)} m_f - \nu_{12} \right] (\sigma_{22} + \sigma_{33}) \right| \\
 & + (10\sigma_{12}/G_{12})^2
 \end{aligned} \tag{30}$$

To model matrix failure, a critical plane search must be carried out. The possible critical planes are rotated from the plane  $x_2 - x_3$  and the “(23)” index is used to describe the stress components in this plane. Now, considering the plane  $x_1 - x_2^{(23)}$ , where the stresses  $\sigma_{11}$ ,  $\sigma_{12}^{(23)}$ ,  $\sigma_{22}^{(23)}$  and  $\sigma_{23}^{(23)}$  are acting, and treating the shear components as a vector, the “effective” shear stress in this plane is [42]

$$\sigma_{12}^\Phi = \sqrt{[(\sigma_{12}^{(23)})^2 + (\sigma_{23}^{(23)})^2]} \tag{31}$$

The index  $\Phi$  is adopted because the following equation can be defined

$$\Phi = a \tan \left[ \sigma_{12}^{(23)} / \sigma_{23}^{(23)} \right] \tag{32}$$

Based on this definition as basis, the tensile and compressive functions used to model the matrix failure are

$$f_P^{(m,c)} = (\sigma_{12}^\Phi / S_{12}^\Phi)^2 + 2(p_\Phi^c / S_{12}^\Phi) \sigma_{22}^{(23)} + (\sigma_{11} / X_{11})^n \tag{33}$$

$$\begin{aligned}
 f_P^{(m,t)} = & (\sigma_{12}^\Phi / S_{12}^\Phi)^2 + 2(p_\Phi^t / S_{12}^\Phi) \sigma_{22}^{(23)} \\
 & + (1 - 2p_\Phi^t S_{22}^t / S_{12}^\Phi) (\sigma_{22}^{(23)} / S_{22}^t)^2 + (\sigma_{11} / X_{11})^n
 \end{aligned} \tag{34}$$

where  $X_{11} = 1.1S_{11}^t$  if  $\sigma_{11} \geq 0$  and  $X_{11} = -1.1S_{11}^c$  if  $\sigma_{11} < 0$ , and  $n$  is a parameter to be experimentally calibrated.

According to Puck and Schürmann [44],  $n$  is typically between 6 and 8. This study uses  $n = 8$ .  $S_{12}^\Phi$ ,  $p_\Phi^c$  and  $p_\Phi^t$  are explicitly defined by Deuschle and Puck [45].

### 2.2.3 LaRC05 criterion

LaRC05 is more recent than the previous models, which have been available for a long time, but it has shown a good potential to predict composite failure. Although Pinho et al. [48] considered nonlinear variations of  $E_2$  and  $G_{12}$  depending on the strain level, this criterion is adapted here to just describe linear stress–strain relations, since they are usually enough for FPF analysis purposes. For shear loads, the nonlinear behavior is more pronounced and usually can be modeled by a hyperbolic tangent curve [35]. However, the assumption of linearly elastic shear model is usually acceptable for FPF analysis. For matrix failure, the theory developed by Puck is used as basis. Assuming that brittle materials are more sensitivity to traction than to compression, the matrix failure is described by

$$\begin{aligned}
 f_L^{(m)} = & \left[ \sigma_{12}^{(23)} / (S_{12} - b_L \sigma_{22}^{(23)}) \right]^2 + \left[ \sigma_{23}^{(23)} / (S_{23}^{(23)} - b_T \sigma_{22}^{(23)}) \right]^2 \\
 & + \left[ \max \{ 0, \sigma_{22}^{(23)} \} / S_{22}^t \right]^2
 \end{aligned} \tag{35}$$

When the normal stress is positive, the term  $\max\{0, \sigma_{22}^{(23)}\}$  considers the break of polymeric chains in tension. This model thus considers mesoscale effects at a macroscale analysis level. In Eq. (35),  $b_L$  and  $b_T$  must be experimentally calibrated and  $S_{23}^{(23)}$  is the shear strength in the plane  $x_1 - x_2^{(23)}$ . According to Pinho et al. [48–50], in transverse compression tests the critical angle  $\theta_0$  is usually between  $51^\circ$  and  $55^\circ$ . Considering  $\theta_0$  as a material property

$$b_T = -(1/\tan 2\theta_0) \tag{36}$$

$$S_{23}^{(23)} = S_{22}^c \cos \theta_0 (\sin \theta_0 + \cos \theta_0 / \tan 2\theta_0) \tag{37}$$

Notice that this prediction for  $S_{23}^{(23)}$  is different from Puck’s. In the absence of additional experimental data,  $\theta_0 = 53^\circ$  and  $b_L = 0.082$  may be used. For tensioned fibers, the traditional maximum stress criterion is adopted

$$f_L^{(f,t)} = \sigma_{11} / S_{11}^t \tag{38}$$

For fibers under compression, two different failure mechanisms may occur: kinking and splitting. However, keeping the focus in linear analyses, just one equation is necessary to model both, since these mechanisms need to be described by different models only for evaluations of the damage progression, not for first-ply failure. If all the fibers are aligned, a rotation by an angle  $\phi$  along the plane  $x_2 - x_3$  must be used to search the critical plane that maximizes the damage function. Once it is found, the plane  $x_1 - x_2^{(\phi)}$  should be analyzed. Fibers misalignment is an intrinsic initial imperfection (from fabrication process, for example), and it must be considered in the failure criterion. Hence, when compression failure mechanisms are analyzed, this initial misalignment contributes significantly for fiber instability due to the initial deformed shape, and another transformation at the plane  $x_1 - x_2^{(\phi)}$  is necessary to consider the stress components with the fiber misaligned direction. The failure function on the misaligned plane can be expressed as

$$f_L^{(f,c)} = \left[ \sigma_{12}^{(mis)} / (S_{12} - b_L \sigma_{22}^{(mis)}) \right]^2 + \left[ \sigma_{23}^{(mis)} / (S_{23}^{(mis)} - b_T \sigma_{22}^{(mis)}) \right]^2 + \left[ \max\{0, \sigma_{22}^{(23)}\} / S_{22}^t \right]^2 \tag{39}$$

Equation (39) is the failure function used by the LaRC05 criterion to define the failure resultant from the load on the longitudinal direction. Even when a pure longitudinal compression is applied (without shear), it is a hard task to define which constituent fails initially. According to Pimenta et al. [51], the following sequence of failure events is expected. First, the material has an elastic behavior even

on the misaligned region. Then, when the load increases, the matrix yields in some points due to the high bending condition, increasing the fiber misalignment angle as rotation in a softer material. Finally, the fiber fails because of excessive small curvatures. Hence, the fiber and matrix failure are closely related, and, in general, it is not possible to affirm which one takes place first. However, it is expected that the matrix yields first. Nevertheless, to avoid misunderstanding, everywhere fiber failure in compression is mentioned in relation to the LaRC05 model, it is just meant that Eq. (39) is equal to 1.

### 3 Results and discussion

In the following analyses, an AS carbon/epoxy composite lamina with properties listed in Table 1 [52] is used for all the simulations. Since the laminas are transversally isotropic,  $E_3 = E_2$ ,  $G_{13} = G_{12}$ ,  $S_{33}^t = S_{22}^t$ ,  $S_{33}^c = S_{22}^c$  and  $S_{13} = S_{12}$ .

#### 3.1 Influence of the lamina orientation in a laminate with a circular hole

Before analyzing stress concentration issues, it is helpful to evaluate the influence of the lamina orientation with respect to the uniaxial load direction on its first-ply failure (FPF) strength to get a better understanding about its failure process. Considering the laminates  $[\alpha]_n$  and  $[\pm \alpha]_{ns}$ , their tensile ( $S_{FPF}^t(\alpha)$ ) and compressive ( $S_{FPF}^c(\alpha)$ ) strength variations according to the fiber-to-load angles predicted using Tsai–Wu, Puck, and LaRC05 criteria are plotted in Fig. 2. This figure considers the stress concentration effects induced by a circular hole in a very large laminated orthotropic plate

**Table 1** Mechanical properties of the AS carbon/epoxy composite used for the simulations [52]

AS carbon/epoxy		
Properties	Units	
$E_1$	GPa	140
$E_2$	GPa	10
$G_{12}$	GPa	6
$G_{23}$	GPa	3.35
$\nu_{12}$	–	0.3
$\nu_{23}$	–	0.49
$E_1^{(f)}$	GPa	231
$\nu_{12}^{(f)}$	–	0.2
$S_{11}^t$	MPa	1990
$S_{11}^c$	MPa	1500
$S_{22}^t$	MPa	38
$S_{22}^c$	MPa	150
$S_{12}$	MPa	70
$S_{23}$	MPa	50

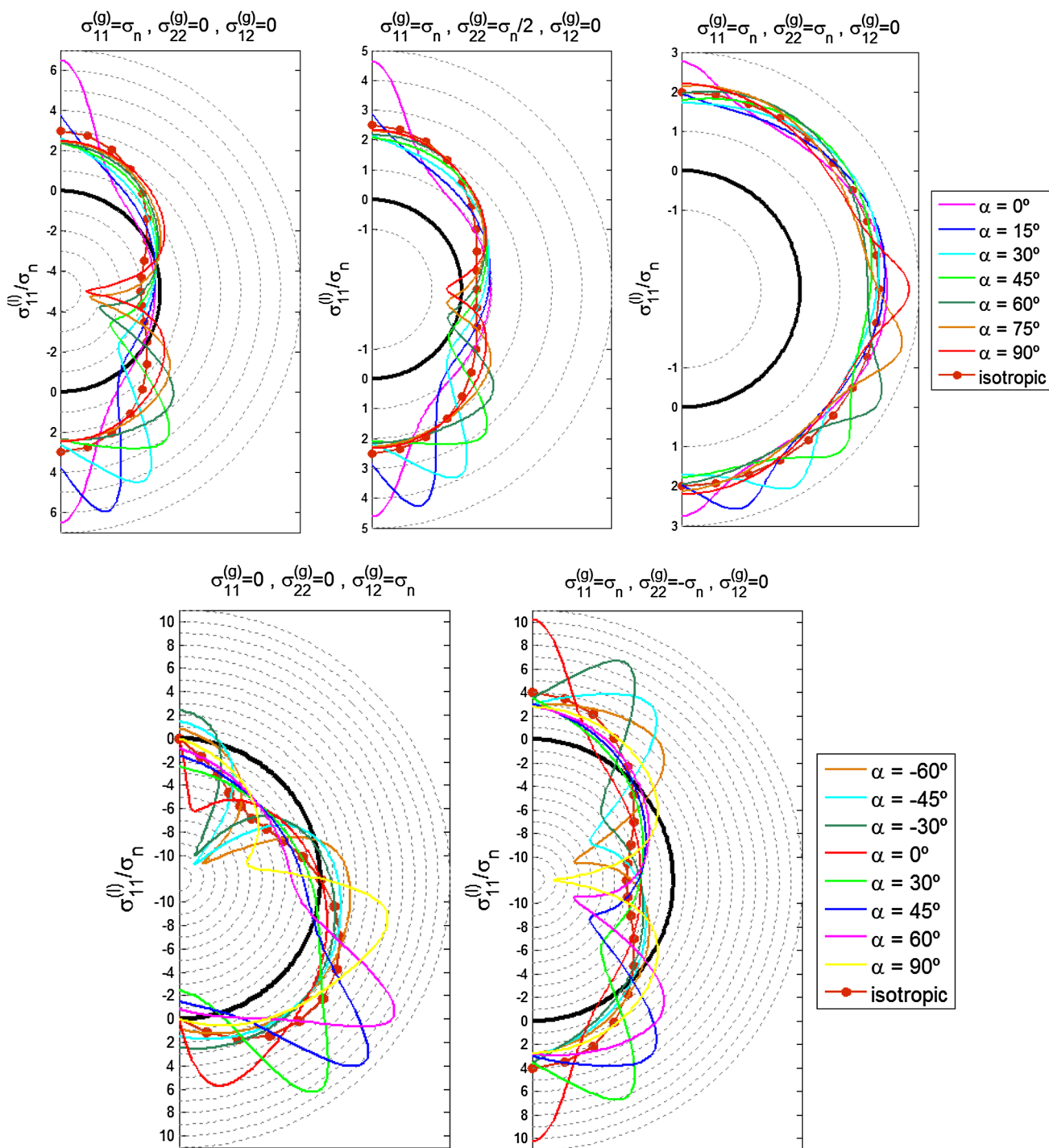


**Fig. 2** Ratio between the tangential stress distribution around the circular hole border and the nominal load  $\sigma_{11}^{(l)}/\sigma_n$  for a large orthotropic plate with a circular hole for different values of  $\alpha$  loaded under vari-

ous loading conditions (notice the two different  $\alpha$  legends, the upper one applicable to the first three figures and the bottom one for the last two)

of the type  $[\alpha]_n$ , with its fiber angle  $\alpha = 0^\circ, 15^\circ, \dots, 90^\circ$  with respect to the main nominal load direction, presented in Fig. 2 for some important load cases, where the thick black line illustrates the hole border. Comparing these results

with those for isotropic materials, it is necessary to point out some important differences:

- (i) for a uniaxial tensile nominal load  $\sigma_{11}^{(g)} = \sigma_n$  (applied on the horizontal direction in the figure), the tangen-

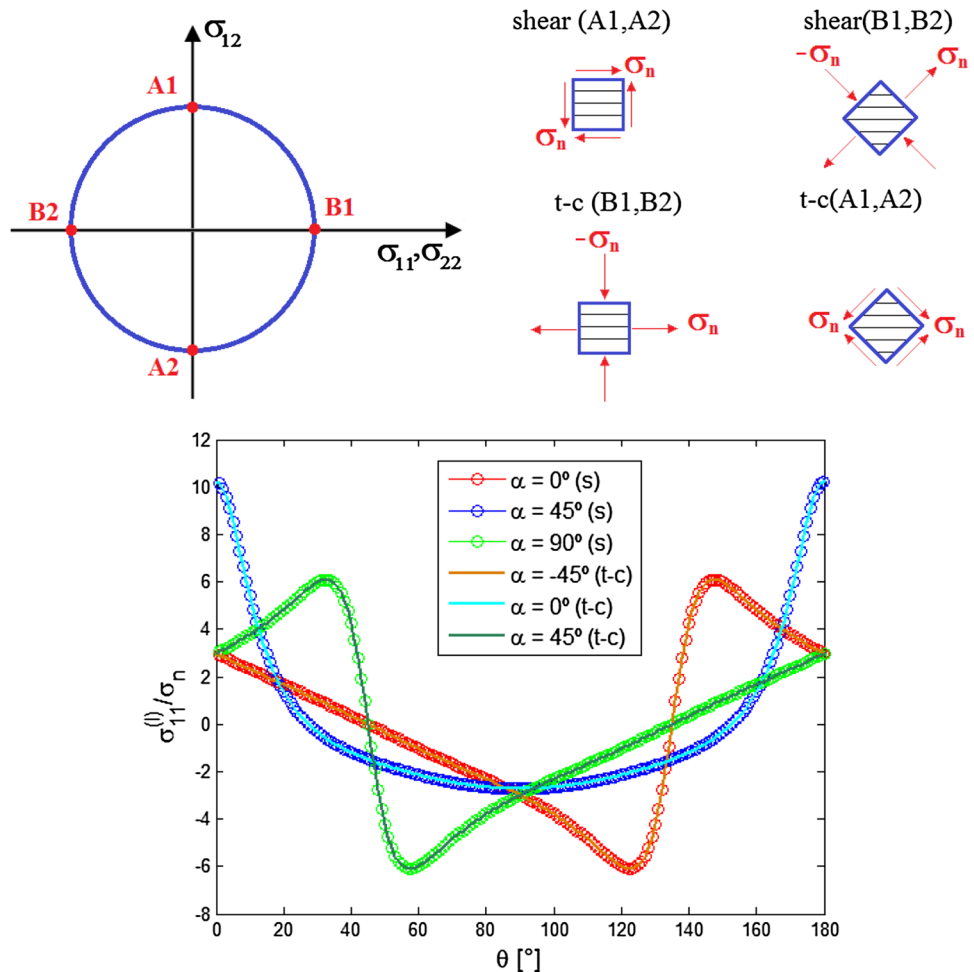
tial or hoop stress distribution along the hole border varies from  $-4 \sigma_n$  up to almost  $7 \sigma_n$ , whereas for isotropic materials this range is between  $-1 \sigma_n$  and  $3 \sigma_n$ ;

- (ii) for nominal stresses in thin-walled pressure vessels  $\sigma_{11}^{(g)} = 2 \cdot \sigma_{22}^{(g)} = \sigma_n$ , the hoop stresses along the hole border can be higher than  $4 \sigma_n$  and can also be even compressive, whereas for isotropic materials the stress along the border is always tensile and ranges from  $0.5$  to  $2.5 \sigma_n$ ;
- (iii) for equal biaxial nominal stresses, there is a small variation on the hoop stress distribution along the hole border, whereas for isotropic materials it is constant and equal to  $2 \sigma_n$ ;
- (iv) for isotropic materials, biaxial tension/compression ( $\sigma_{11}^{(g)} = \sigma_n, \sigma_{22}^{(g)} = -\sigma_n$ ) and pure shear loads are equivalent and induce a stress concentration factor  $4 \sigma_n$ , whereas for anisotropic materials the effects of these loads are significantly different, as shown in the lower figures, because of the asymmetry induced by the fibers, a non-intuitive result.

The difference between the pure shear (s) and equal tension–compression (t–c) behavior in this very large orthotropic plate with a central circular hole is due to the influence of the fibers direction on the stress concentration effects. Figure 3 shows the Mohr’s circle, which is equal for both (s) and (t–c) loads, and a differential element with  $\alpha = 0^\circ$ , for simplicity. The stress concentration along the hole border is similar, as it should be, but it acts on material elements with fibers rotated  $45^\circ$ . Consequently, although the shear strength can be obtained from a tension–compression test, the tested strength represents the case of pure shear acting in an orthotropic plate with a different fibers orientation.

Therefore, to apply a failure criterion to predict the stress concentration effect on the orthotropic plate, it is necessary to transform the stress components from a local system, tangent to the border, to a material coordinate system, which coincides with the fibers direction. For uniaxial loads, the material stresses around the circular hole border are presented in Fig. 4 for various fibers-to-load angles  $\alpha$ , as a function of the point location around the hole border  $\theta$ . Predictions of tensile and compressive FPF strengths for these cases by the three failure criteria used in this work

Fig. 3 Different stress concentration effects under pure shear and equal tension–compression loads



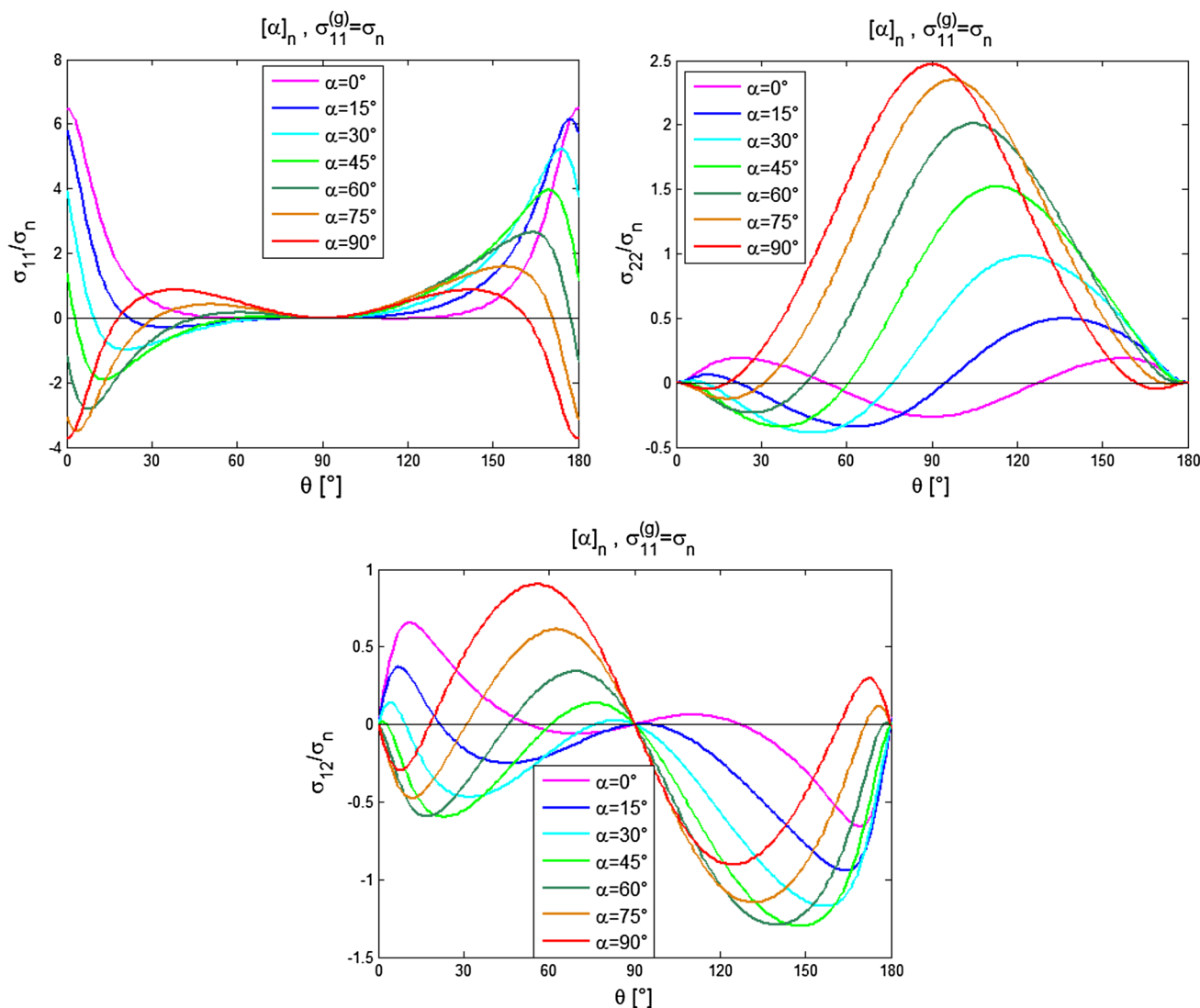


Fig. 4 Stresses around the circular hole border in material coordinates for uniaxial loads

are shown in Fig. 5, as a function of the fibers orientation. For tension loads, the three failure theories yield quite close results, while for compression loads they generate significantly different predictions. The results are normalized by the strengths of unnotched laminates on the fibers direction. For convenience, FPF is used to denote the initial damage of the plate henceforward, even knowing that it does not mean total failure of the first ply.

Despite the drastic notch-induced reduction in the predicted FPF strength for the studied orthotropic plate, this result can be easily explained. Notice in Table 1 that  $S_{11}^t/S_{22}^t = 52.4$  and  $S_{11}^c/S_{22}^c = 10$ , an indication that matrix failure tends to be the dominant mechanism in Fig. 5. To further explore this result, the failure functions are studied along the circular hole border for some selected fiber inclinations and applied stress levels. So, three different loading

conditions are analyzed next (namely  $\sigma_{11}^{(g)} = 90$  MPa and  $\alpha = 0^\circ$ ;  $\sigma_{11}^{(g)} = -70$  MPa and  $\alpha = 15^\circ$ ; and  $\sigma_{11}^{(g)} = -60$  MPa and  $\alpha = 75^\circ$ ), to illustrate the difference in the FPF predictions made by the three studied anisotropic failure criteria.

For pure tensile loads aligned with the fibers, with  $\alpha = 0^\circ$ , all models predict that the FPF failure initiates for  $90 \text{ MPa} < \sigma_{11}^{(g)} < 100 \text{ MPa}$ . Because Puck and LaRC05 use separate matrix and fiber failures models, their predictions for each component are presented, and for this case matrix failure is expected for all cases, see Fig. 6 (although the load is not high enough to cause it, since in all cases  $f < 1$ , whereas failure occurs when  $f = 1$ ). However, contrary to what happens in isotropic plates, failure is expected in this case at  $\theta \cong \mp 20^\circ$ , instead of at  $\theta = 0^\circ$ , even though the maximum stress concentration point is  $\theta = 0^\circ$  (see Fig. 2). Therefore, it is worth to point out once again that the critical stress

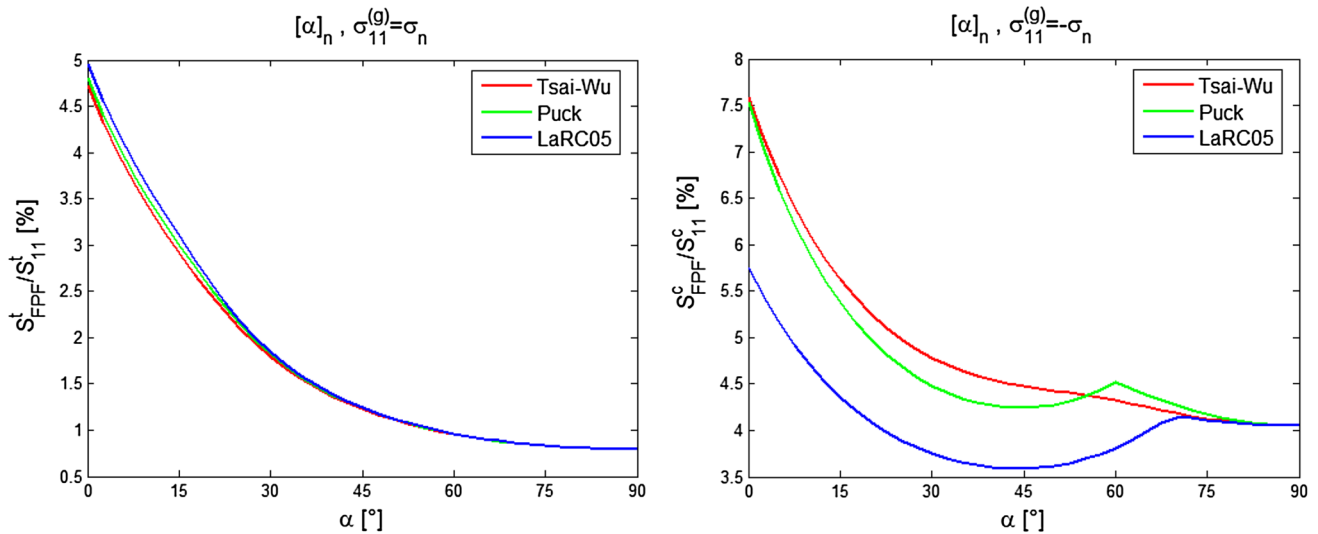


Fig. 5 Prediction of  $S_{FPF}^t/S_{11}^t$  and  $S_{FPF}^c/S_{11}^c$  for the holed orthotropic plate strength for initial damage under tension and under compression loads by the 3 failure criteria, as a function of the fibers-to-load angle  $\alpha$

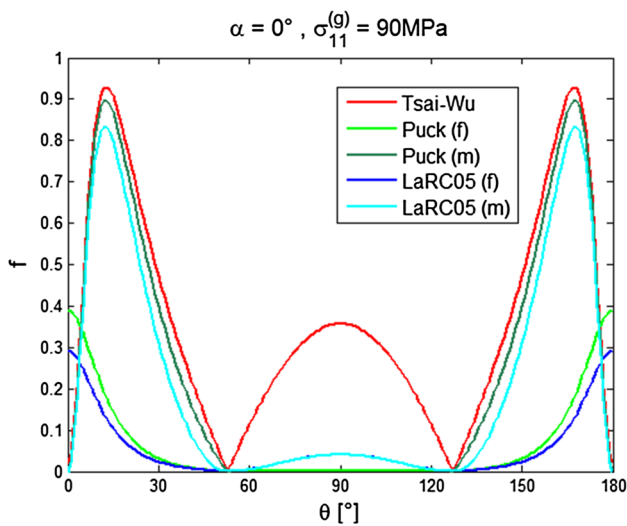


Fig. 6 FPF tendency predicted by the three damage criteria for the orthotropic plate with a circular hole loaded by a pure tensile load  $\sigma_{11}=90$  MPa aligned with its fibers (since failure is predicted when  $f=1$ , none of the criteria predicts failure in this case, but it is expected under slightly higher loads in the matrix, at a position  $\theta \cong \pm 20^\circ$ )

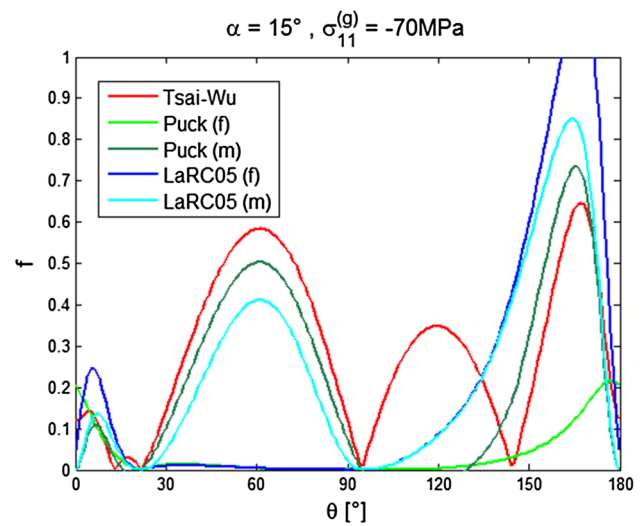


Fig. 7 FPF tendency predicted by the three damage criteria for the holed orthotropic plate loaded under a compressive load of  $-60$  MPa that makes an angle  $\alpha=15^\circ$  with its fibers direction. Failure is predicted in the fibers by the LaRC05 criterion, but not by the Puck and the Tsai–Wu criteria

concentration point is not the most stressed point along the hole border in this notched anisotropic plate.

Figure 7 shows the FPF prediction for the same orthotropic large plate with a circular hole under a uniaxial pure compressive load  $\sigma_{11} = -70$  MPa, when the fibers make an angle  $\alpha = 15^\circ$  with the load direction. In this case, the difference between the various anisotropic failure criteria predictions is significant. Just the LaRC05 model predicts fiber failure at the location  $\theta \cong 170^\circ$ . Moreover, the precise

position of the critical point around the hole border predicted by the three criteria is not identical, neither it coincides with the critical point for isotropic plates. Only the LaRC05 criterion indicates fiber failure under compression for this case, because this model is the only one where fiber instability failure is considered, as discussed in Sect. 2.

Figure 8 shows the FPF tendency prediction for the same holed orthotropic plate under a uniaxial compressive load of  $-60$  MPa, when the fibers make an angle  $\alpha = 75^\circ$  with the

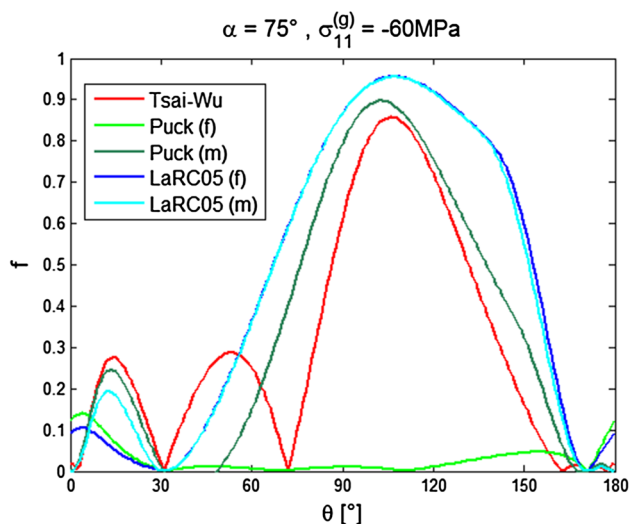


**Fig. 8** FPF predicted by the three damage criteria for the holed orthotropic plate loaded under a compressive load of  $-60$  MPa that makes an angle  $\alpha = 75^\circ$  with its fibers direction

load direction. The difference between the various failure criteria predictions in this case is also significant. No criteria predicts failure, but all of them indicate that the critical point around the hole border is  $\theta \cong 100^\circ$ , again at slight different points, at a position quite different from that predicted for isotropic plates. It is interesting to note that LaRC05 predicts an equal tendency for failure of the fibers and of the matrix, whereas Puck predicts that the fibers are much more resistant than the matrix. Hence, in the authors opinion, these compressive load cases could be a good test to verify which of these criteria can better describe the behavior of such holed orthotropic plates, despite the practical difficulty to test thin holed plates in compression.

The stress distributions in material coordinates along the circular hole border induced by applied pure shear loads are presented in Fig. 9 for large orthotropic plates with various fiber-to-load angles  $\alpha$ . For the orthotropic material whose properties are listed in Table 1, these stress ratios vary significantly with  $\alpha$ . Note in particular that  $\sigma_{11}/\sigma_n$  may reach much higher values than the isotropic  $K_r$ , information that cannot be neglected when designing notched orthotropic plates. Once again, these results are not intuitive, at least for structural engineers trained to dimension notched plates of isotropic materials.

For isotropic materials, pure shear is equivalent to equal biaxial tension/compression and induce maximum and minimum stresses  $\pm 4 \sigma_n$ , since the corresponding values for pure tension are  $3 \sigma_n$  and  $-1 \sigma_n$  and the superposition principle may be directly used in these materials. On the other hand, for anisotropic materials, even for the elastic regime, it is necessary to take special care before applying the superposition principle: the stress must be defined in the

material coordinate system, because the same load has different effects for different fiber-to-load angles. For example, considering a pure shear load  $\sigma_{12}^{(g)} = \sigma_n$  with a general fibers-to-load angle equal to  $\alpha$ . The superposition principle can be used to compute the effect of a tensile load with  $\sigma_{11}^{(g)} = \sigma_n$  and a compressive load with  $\sigma_{22}^{(g)} = -\sigma_n$ , both with fibers-to-load angle equal to  $\alpha - 45^\circ$  (or, in a similar way,  $\sigma_{11}^{(g)} = -\sigma_n$  and  $\sigma_{22}^{(g)} = \sigma_n$  and fibers-to-load angle equal to  $\alpha + 45^\circ$ ), as it is clearly shown in Fig. 3 by Mohr's circle. The superposition principle is a fundamental tool to model mechanical systems and may be applied for any material, while it is in its linear and elastic range. The single fundamental condition to apply the superposition principle is that a given solicitation must be linearly related to the structural response, independently of any kind of anisotropy.

The FPF strength predictions for the large orthotropic plate with a circular hole when it is loaded by pure nominal shear stresses are presented in Fig. 10. These predictions have two distinct phases: if  $40^\circ < \alpha < 50^\circ$ , then the FPF models estimate a peak strength almost constant and equal to about  $0.78 S_{12}$ , where  $S_{12}$  is the strength measured in an unnotched specimen listed in Table 1; else, the strength presents a smooth decrease, reaching a minimum for  $\alpha = -45^\circ$ . The tension/compression strengths are not plotted to avoid repeated information, since it has just a fiber-to-load angle shift of  $45^\circ$ . However, using the same argument based on the superposition principle for the shear and for the tension/compression loads analogy, the anisotropic strength predictions can be better interpreted. The FPF strength of the large notched orthotropic plate is maximized when the maximum tensile stress is acting parallel to the fibers direction ( $\alpha = 45^\circ$  for pure shear and  $\alpha = 0^\circ$  for tension or compression), and it is minimized when the tensile stress acts in the matrix direction ( $\alpha = -45^\circ$  for pure shear and  $\alpha = \pm 90^\circ$  for the tension/compression case).

The tensile and compressive FPF strengths can yield values smaller than 8% of the properties of the unnotched plate, but these values are normalized by strengths on the fibers direction, which are much higher than the matrix properties (recall that  $S'_{11}/S'_{22} = 52.4$  and  $S^c_{11}/S^c_{22} = 10$ ). On the other hand, the failure of a large plate loaded by pure shear ranges from 20% up to almost 80% of the unnotched strength. The reason for this prediction is because the failure of notched plates is dominated by the matrix in the majority of the cases studied, as well as the failure for the unnotched plate under shear. This is why the shear strength ratio is not so notch-sensitive, contrary to the tensile and compressive strengths that were normalized using the properties on the fiber direction. Two different cases are selected to evaluate the different predictions made by the various failure criteria for pure shear loads:  $\sigma_{12}^{(g)} = 42.5$  MPa and  $\alpha = 30^\circ$ ; and  $\sigma_{12}^{(g)} = 50$  MPa and  $\alpha = 45^\circ$ . Figure 11 shows the failure functions values for a shear load of 42.5 MPa when the fiber-to-load angle is  $30^\circ$ .

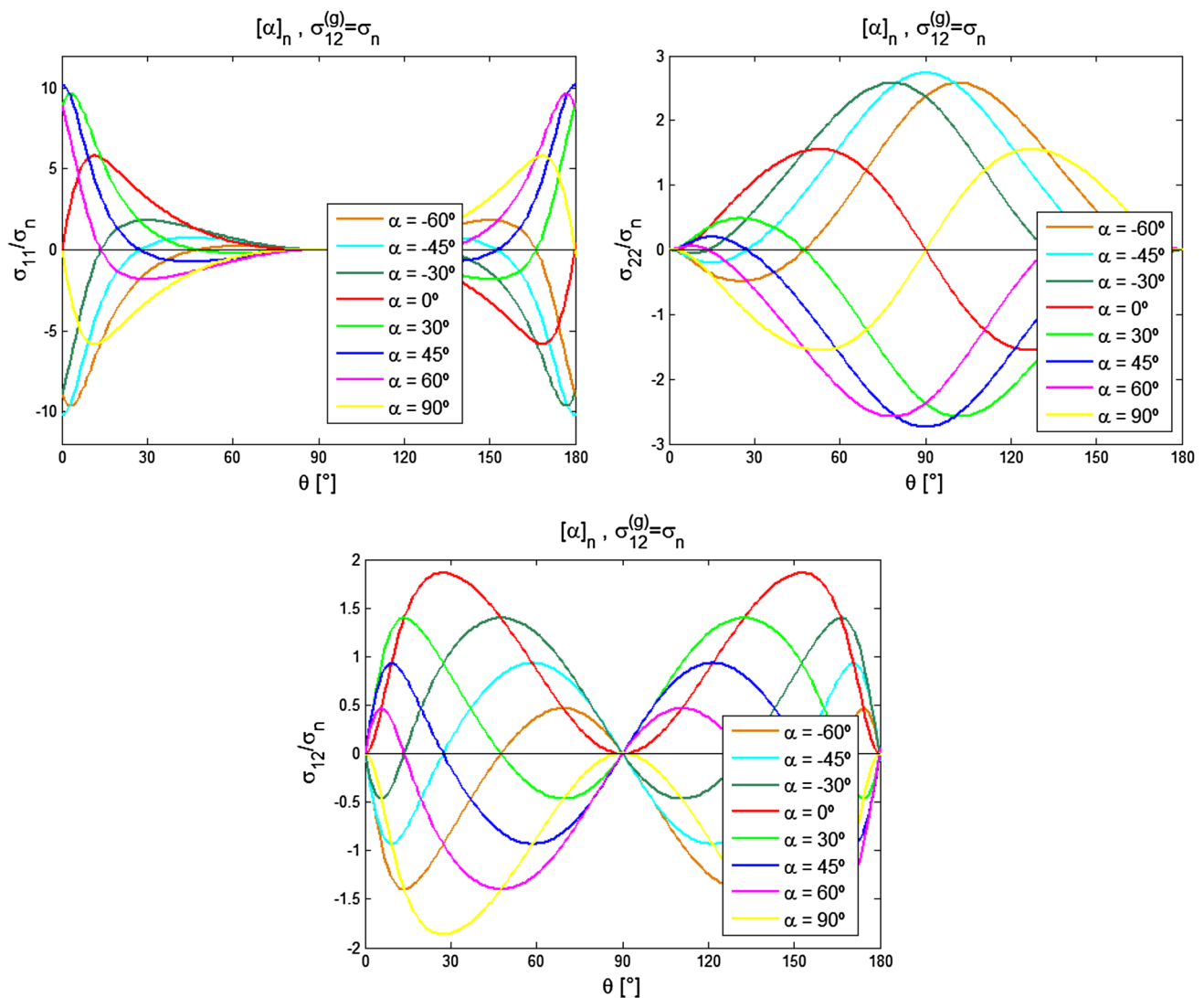


**Fig. 9** Material stress distributions along the circular hole border induced by pure nominal shear loads for various fiber-to-load angles  $\alpha$  in a large plate of the orthotropic material whose properties are listed in Table 1

Despite the difference of the predicted damage distributions along the hole border position  $\theta$ , the estimates of the critical point are similar,  $\theta \cong 20^\circ$  (except for fibers that fail according to the LaRC05 criterion, but this model predicts that the matrix fails before the fiber in this case). These plots also show a tendency that can be extended to the other graphics: for matrices under tension, Tsai–Wu predicts earlier FPF, while for matrices under compression, Tsai–Wu predicts the smallest value of the failure index. Notice in Fig. 11 that failure is predicted by the Tsai–Wu criterion, but not by the Puck and the LaRC05 criteria.

Figure 12 shows the FPF prediction for an applied shear stress of 50 MPa when the fibers make an angle  $\alpha = 45^\circ$  with the load direction, which presents the highest strength for pure shear (see Fig. 10). For this load level, although none

of those criteria indicates failure, some conclusion still can be pointed out analyzing their tendency. Once again, the difference between the fibers failure prediction under compression made by Puck and LaRC05 is quite large: while Puck estimates  $f < 0.1$  for  $\theta = 90^\circ$ , LaRC05 predicts  $f \cong 0.9$ , making necessary an experimental validation of the hypotheses assumed during each model formulation.

Notice in Fig. 12 that no criterion predicts failure, but all of them indicate that the critical point around the hole border is  $\theta \cong 90^\circ$ . Notice as well that LaRC05 predicts an equal tendency for failure of the fibers and of the matrix, whereas Puck predicts that the fibers are much more resistant than the matrix (it is equivalent to  $\sigma_{11}^{(g)} = -\sigma_{22}^{(g)} = 50$  MPa and  $\alpha = 0^\circ$ ). This is because the LaRC05 uses a quite similar equation to model matrix and

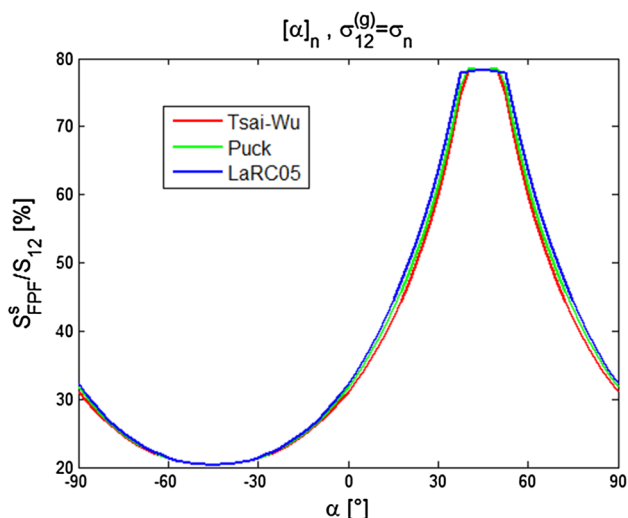


Fig. 10 Prediction of  $S_{FPF}^s / S_{12}$  for the orthotropic plate with a circular hole strength, considering initial damage under pure shear loads by the 3 failure criteria, as a function of the fibers-to-load angle  $\alpha$

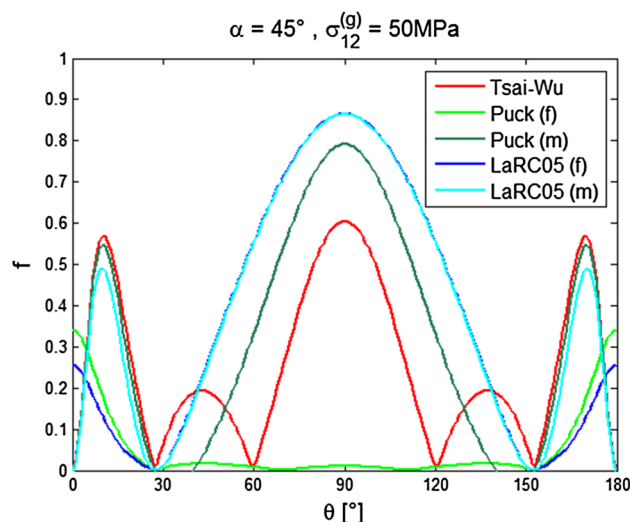


Fig. 12 FPF predicted by the three damage criteria for the holed orthotropic plate loaded under a shear load of 50 MPa that makes an angle  $\alpha = 45^\circ$  with its fibers direction

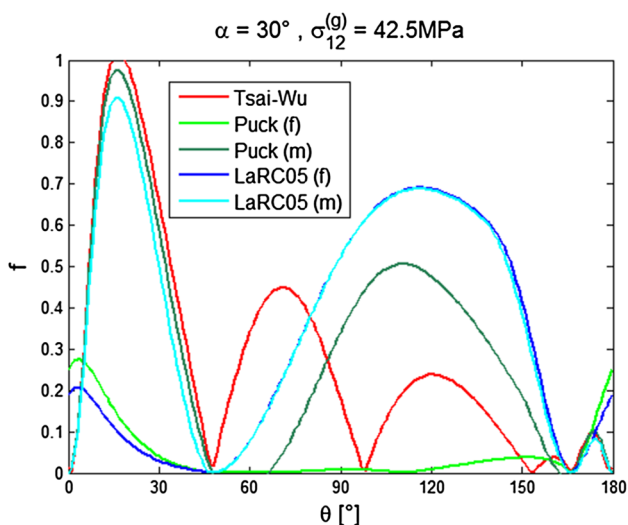


Fig. 11 FPF tendency predicted by three failure criteria for the holed orthotropic plate loaded under a shear load of 42.5 MPa that makes an angle  $\alpha = 30^\circ$  with its fibers direction

fiber under compression; the difference is just the misalignment angle. On the other hand, the Puck model for fiber compression failure just add the last term, to take into account the shear influence on fiber instability, when compared to the tension one. Moreover, for matrix failure, the Puck model also considers the critical plane idea, as well as the LaRC05.

Once the three simplest loads are studied (pure tension, compression, and shear), it is useful to evaluate the effect of multiaxial loads. For this purpose, two different simple biaxial load cases can be studied: tension/tension

and compression/compression. Recall that the tension/compression load is similar to the shear one, but with an angle-to-load shift of  $45^\circ$ . For both, the stress concentration in local coordinate is independent of the value of  $\alpha$ , as shown in Fig. 13, i.e., the strength curves are superposed. This behavior becomes clear using Mohr's circle; the radius of the circle is equal to zero, and hence, no influence of the fiber-to-load angle is realized. All the failure models studied here made exactly equal predictions for biaxial strengths:  $S_{FPF}^{t-t} = 17.7$  MPa and  $S_{FPF}^{c-c} = -68.1$  MPa (hence their plots are omitted). Notice that these values are equivalent to  $S_{FPF}^{t-t} = S_{22}^t / 2.2$  and  $S_{FPF}^{c-c} = -S_{22}^c / 2.2$ , which indicates that the matrix fails under pure tension or compression, justifying why the strength predictions are equal. To prove this affirmation, the failure functions variation along the hole border are evaluated next.

Figures 14 and 15 show that although their FPF tendency distributions along the hole border are different (in particular for compression), the models tend to become coincident when the nominal stresses are close to the predicted strength, since all of them predict failure for  $\theta = 90^\circ$ . According to Fig. 13, the matrix is under pure uniaxial stresses in this point, so failure occurs when the stress in it is equal to the matrix strength. Indeed, all theories must indicate failure when there is just one non-null stress component on the material coordinate system and it equals the equivalent strength in that direction.

From the results presented in Figs. 14 and 15, it can be expected that the matrix starts to fail before the fibers in plates with circular holes, except maybe for fibers under compression according to the LaRC05 model. All these failure theories also predict that uniaxial tension with  $\alpha = 0^\circ$  and pure

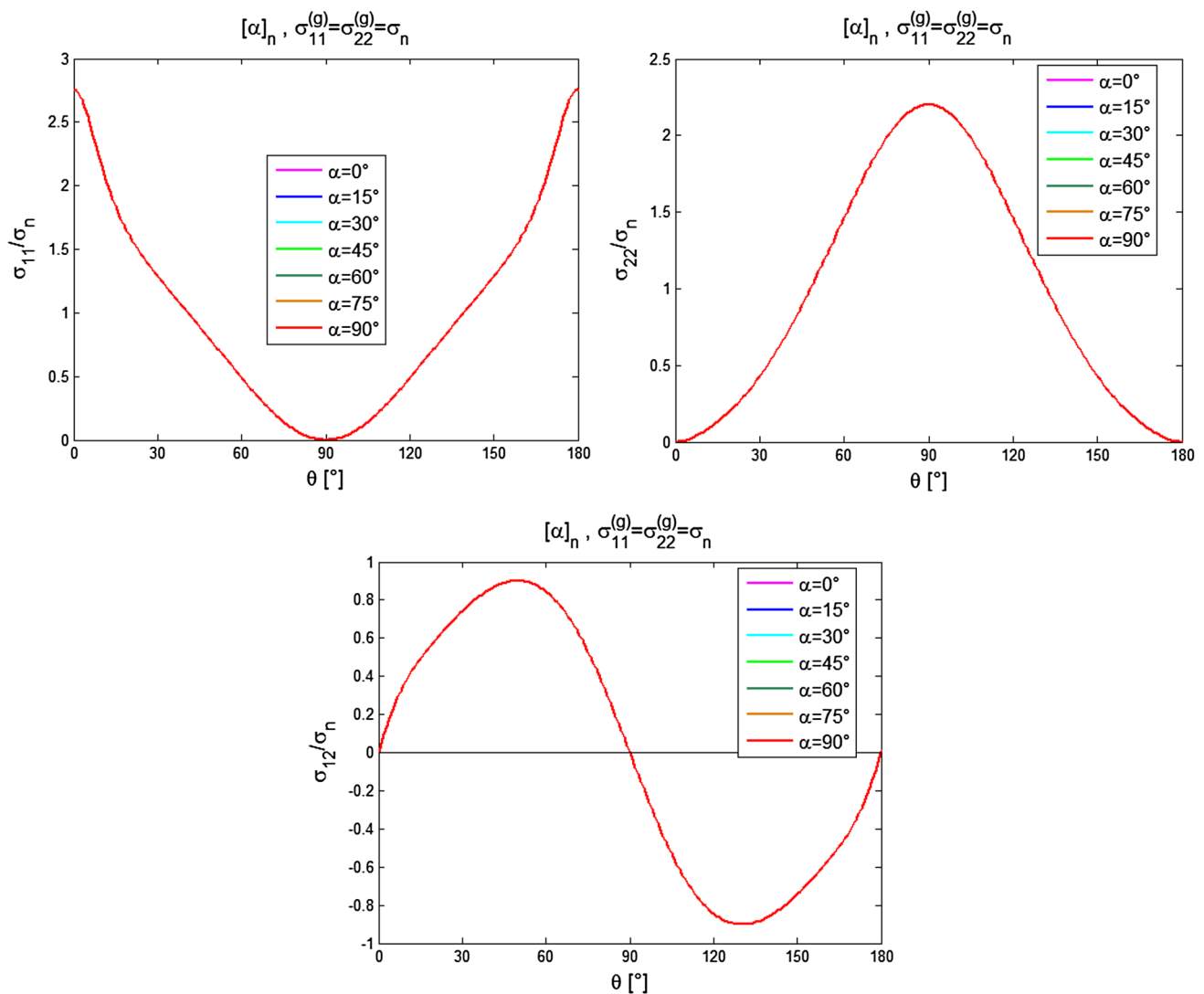


**Fig. 13** Stress concentration distribution in the material coordinate system for biaxial loads

shear with  $\alpha = 45^\circ$  maximize the stress concentration effect. However, because the strengths are dependent on the fiber orientation, to minimize the  $K_t$  value is not necessarily the most important design guideline. Although stress concentrations should be avoided, most real structures need notches for functional reasons. However, contrary to isotropic materials, for the anisotropic plates studied here the most important point is not to minimize  $K_t$ , but instead to minimize its direction-dependent effect on the notched structure. Moreover, the strength decreases for an isotropic large plate with a circular hole is equal to 3 for tensile or compressive loads and equal to 4 for shear, while for the orthotropic laminate the strengths decrease may be much more important depending on the load. Indeed, their strength decreases at least by a factor of 20 for tension, 12.5 for compression, and 1.25 for shear (the results may be even higher according to the fibers orientation). Notice

that for shear loads, the notch effect is less pronounced for unidirectional laminates than for isotropic materials.

The LaRC05 model can underestimate the strength of the holed laminated plates when their fibers fail under compression, if the misaligned fibers do not coincide with the point around the hole. Even though the fiber misalignment is usually smaller than  $5^\circ$ , neglecting this small angle does not result in very different predictions. The main reason for LaRC05 and Puck unmatched estimations for fibers under compression is their phenomenological basis: the LaRC05 criterion attempts to model fiber instability and matrix yielding in a critical plane. Single-layered laminates ( $[\alpha]_n$ ) have limited practical use since their stiffness and strength are too anisotropic, whereas many real loads are multiaxial. Nevertheless, it is important to understand the  $[\alpha]_n$  behavior, since it can be extended to any symmetric laminate using homogenization techniques [53].

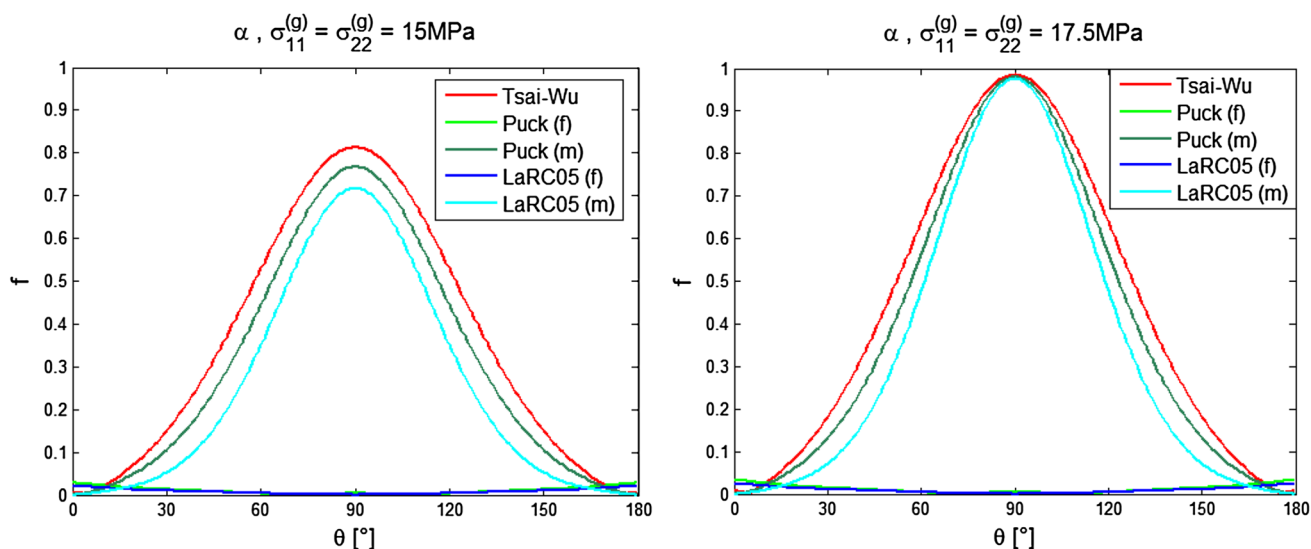


Fig. 14 FPF tendency predicted by the three damage criteria for the orthotropic plate with a circular hole loaded under biaxial tension/tension load of 15 MPa and 17.5 MPa

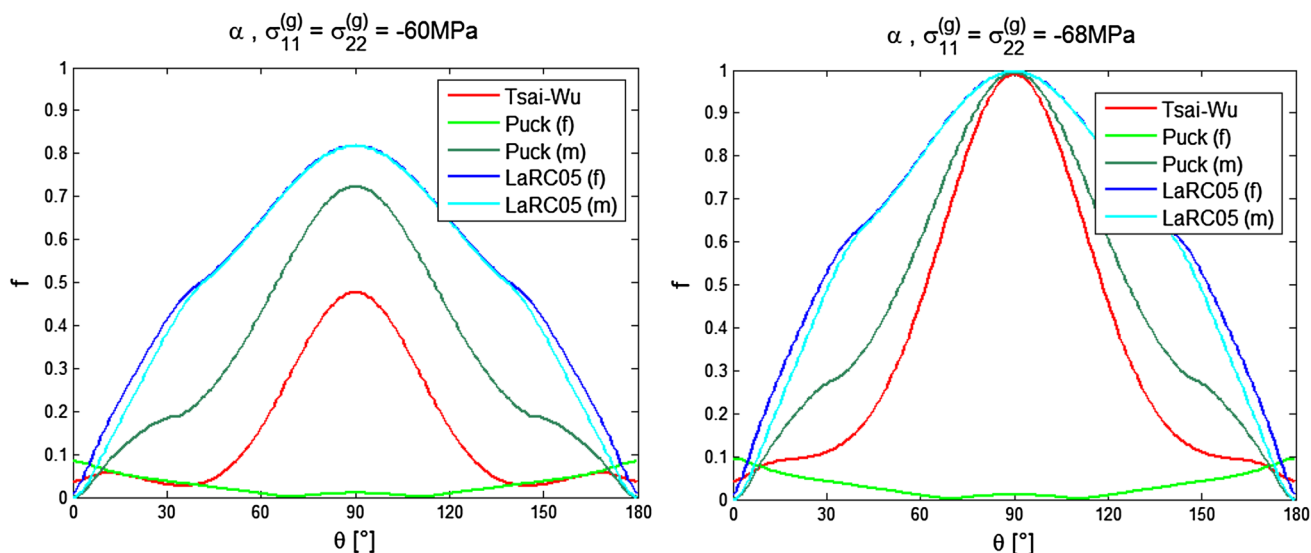


Fig. 15 FPF tendency predicted by the three damage criteria for the orthotropic plate with a circular hole loaded under biaxial compression/compression load of -60 MPa and -68 MPa

### 3.2 Elliptical holes

Two additional variables are needed to analyze the effect of elliptical holes in large single-ply anisotropic plates: the ratio between the ellipse semi-axes  $r_a/r_b$  and the ellipse inclination  $\beta$  in relation to the fibers, see Fig. 1. Although more laborious to analyze, elliptical holes are especially useful to approximate other notches and to study stress gradients and fracture effects [54–58]. Three different ellipse aspect ratios,  $r_a/r_b = 2, 5, 10$ , are analyzed here, but to simplify this study, just uniaxial nominal stress and

single-layered laminates are considered in this section. The scope of this analysis is to evaluate the influence of the ellipse aspect ratio and of its inclination. Before proceeding, notice that sometimes it is useful to plot the data using  $\beta^* = \beta + \alpha$  coordinates, since they may better represent the ellipse inclination effects in relation to the global axes where the load is applied, where  $\beta$  is the elliptical hole inclination in relation to the materials coordinates (see Fig. 1).

Figures 16, 17, and 18 show the stress concentration effects in material coordinates for the laminate  $[\alpha]_n$  with

$r_a/r_b = 2$  and fiber-to-load angles varying from  $0^\circ$  to  $90^\circ$  in  $30^\circ$  steps. To better interpret these results, the same color scale is used for each stress component, independent of the fibers-to-load angle. Figure 16 shows that  $\sigma_{11}$  is maximized for  $\alpha = 0^\circ$ , while the opposite occurs with  $\sigma_{22}$ , which, as expected, is maximized for  $\alpha = 90^\circ$ . Moreover, the most important point from these figures is that the ellipse inclination that maximizes the stress concentration effect in absolute value is not necessarily  $\beta^* = 90^\circ$ , as well known for isotropic materials. Indeed,  $\sigma_{11}$  is maximized when  $90^\circ < |\beta^*| < 90^\circ + \alpha$  ( $90^\circ - \alpha < |\beta^*| < 90^\circ$ ), as well demonstrated for the laminate  $[30]_n$  in Fig. 16, and  $\sigma_{22}$  has a higher magnitude when  $60^\circ < |\beta^*| < 90^\circ$  ( $60^\circ - \alpha < |\beta^*| < 90^\circ - \alpha$ ), e.g., for  $[60]_n$  in Fig. 17. Although  $\sigma_{12}$  also affects failure,  $\sigma_{11}$  and  $\sigma_{22}$  are easier to

physically understand, since these stress components can be easily separated into fiber and matrix components, while  $\sigma_{12}$  jointly affects both matrix and fibers failure mechanisms.

Hwu and Ting [59] proved analytically that under uniaxial loads  $\sigma_{11}^{(g)} = \sigma_n$ , when the ellipse inclination is  $\beta = 90^\circ$ , the stress concentration factor at the tips of the minor elliptical hole axis  $\theta = 90^\circ$ , which for isotropic materials is equal to -1, for anisotropic materials is also independent of the ratio  $r_a/r_b$  and depends only on material properties. However, whereas the  $K_t$  value is sufficient to analyze stress concentration effects in isotropic materials, whose strength is independent of the direction, such a punctual stress solution is not enough to predict the failure of anisotropic materials, which must be analyzed considering the entire stress-to-strength distribution along the notch border.

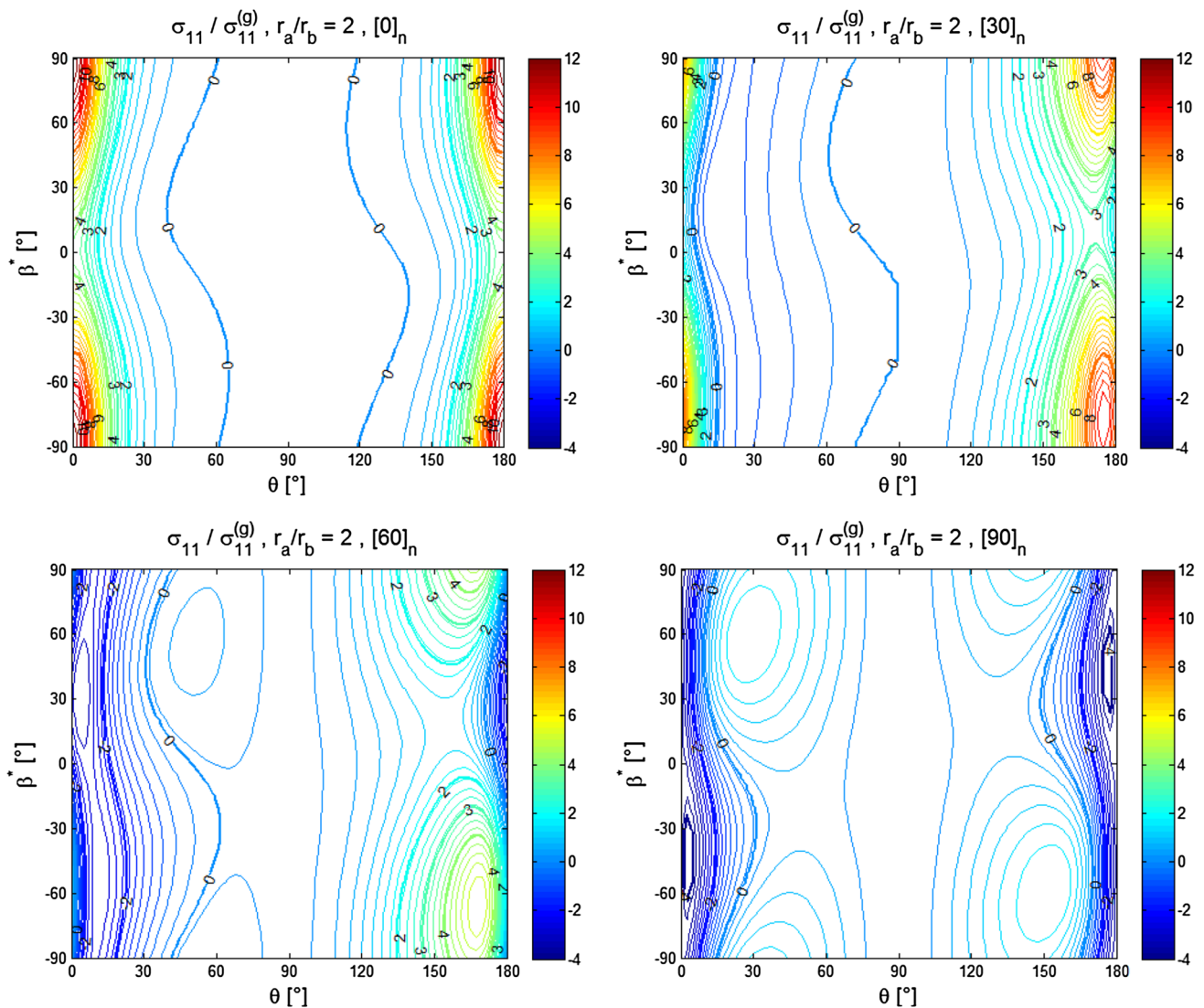


Fig. 16  $\sigma_{11}$  stress concentration for  $[\alpha]_n$  laminated plates with a central elliptical hole with  $r_a/r_b = 2$

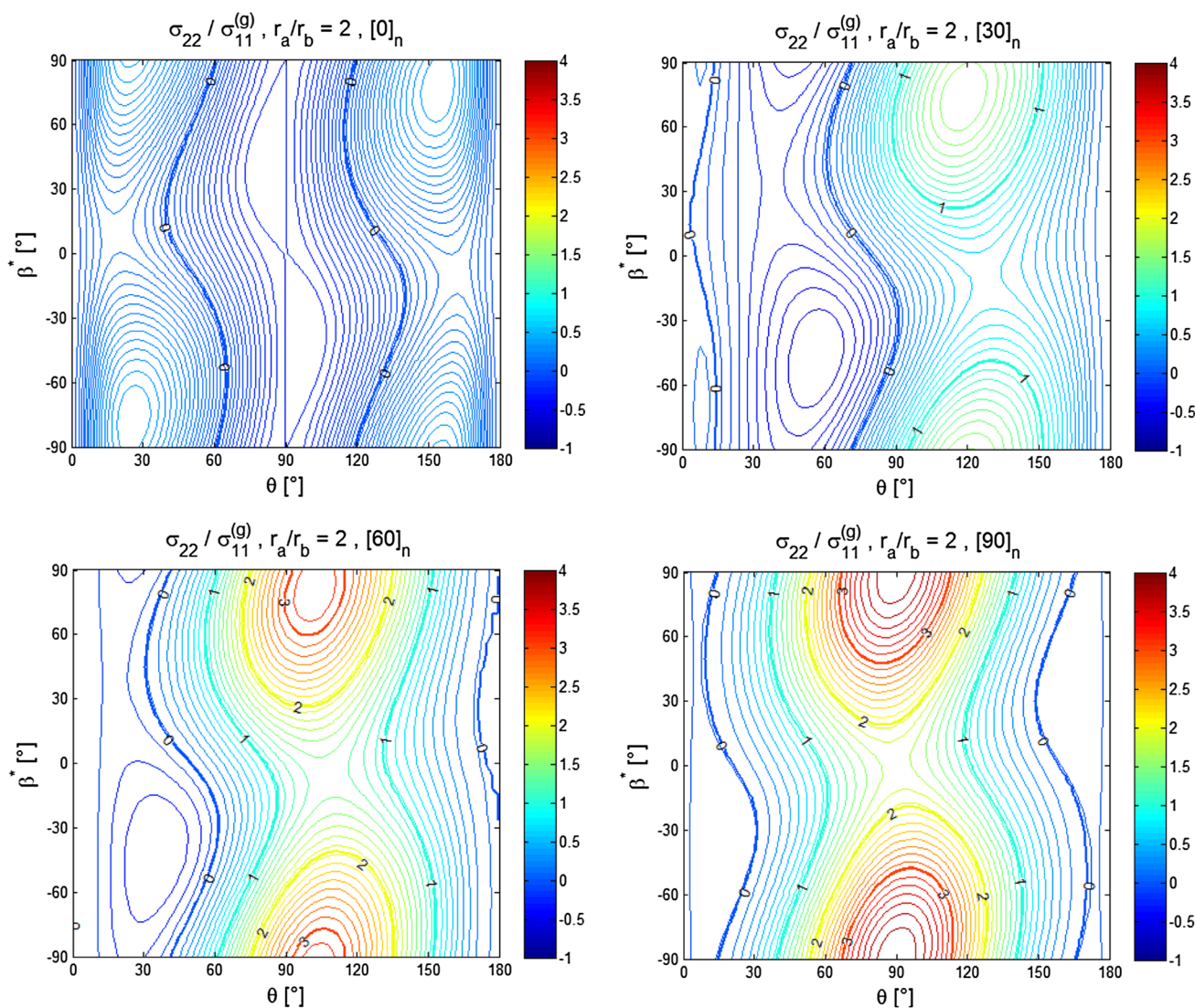
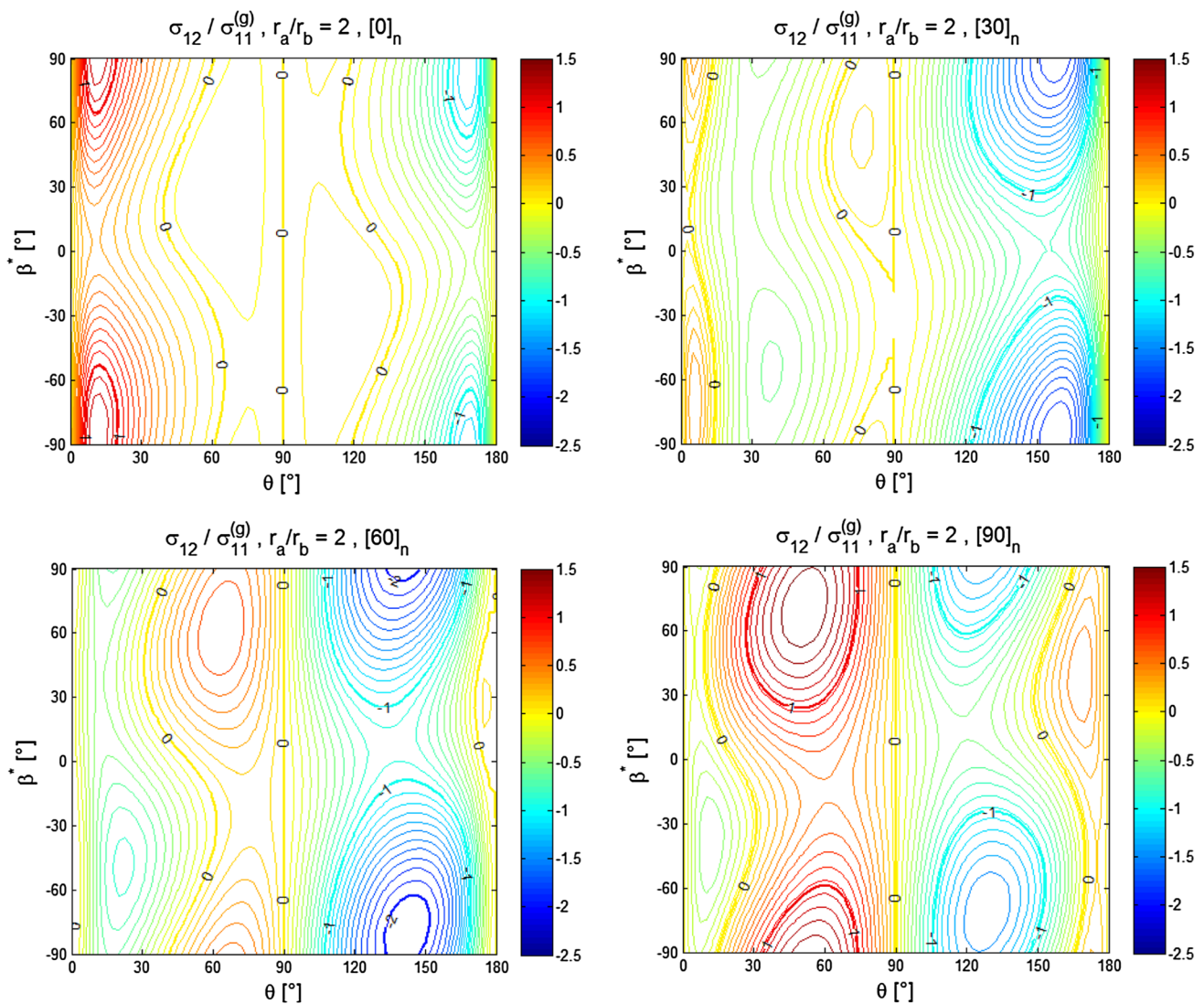


Fig. 17  $\sigma_{22}$  stress concentration for  $[\alpha]_n$  laminates with elliptical hole ( $r_a/r_b = 2$ )

To get a better comprehension about the ellipse geometry and inclination influence on the failure process of a large anisotropic plate, a parametric study of tension and compression loads is presented in Fig. 19, which shows the tensile and compressive strengths, respectively, for the same ranges of fiber-to-load angles presented in Figs. 16, 17, 18. First, it is important to notice the axes scales for the tensile loads. Different scales are needed to permit a good interpretation of all graphics. However, the scale is the same for all compressive strengths predictions. This observation alone is enough to indicate that the tensile strength is more sensitive to the  $r_a/r_b$  ratio than the compressive strength.

Tensile loads with  $\beta = -\alpha$ , for which the ellipse major axis is parallel to the load direction, result in higher FPF strengths. On the other hand, the most critical position is usually around  $90^\circ - \alpha < \beta < 90^\circ$ , for which the major ellipse

axis inclination is between a direction perpendicular to the applied load  $x_2^{(g)}$  and the direction perpendicular to the fibers  $x_2$ . The tendency of damage evolution perpendicular to the fibers if  $\alpha = 0^\circ$  can be understood supposing that the set hole plus damaged zone could be approximated using an elliptical hole and that the ratio  $r_a/r_b$  increases as the damaged zone increases. The difference between the notched plate strength for  $\beta = \pm 90^\circ$  and for the other elliptical hole inclinations also increases with  $r_a/r_b$ . For  $\alpha = 90^\circ$ , the matrix is expected to fail, as clearly shown by the different scales needed for the strength axes, and the same reasoning is valid. Moreover, the large difference between the predicted strengths indicates that matrix failures are expected at least for  $\alpha > 15^\circ$ , a prediction that is in agreement with the experimental results presented by Kaman [9] to evaluate fracture in  $[0/\theta]_s$  laminates using a fracture mechanics approach.



**Fig. 18**  $\sigma_{12}$  stress concentration for  $[\alpha]_n$  laminates with elliptical hole ( $r_a/r_b = 2$ )

For compression loads, a similar strength behavior is presented and the tendency of the LaRC05 model to estimate failure before the other models decreases when  $r_a/r_b$  increases, because of the critical point location. Moreover, for  $\beta = 0^\circ$  all the three models yield very similar predictions and the notched strength is almost independent of the ratio  $r_a/r_b$ . To help understanding the failure mechanism, Fig. 20 shows the variation of the notched compressive strength according to  $r_a/r_b$ , Fig. 21 shows the stress concentration, and Fig. 22 shows the failure functions. Tsai–Wu and Puck models indicate that the strength is constant for  $r_a/r_b > 1.4$  and LaRC05 for  $r_a/r_b/2$  (see Fig. 20). The stress distribution around the hole, presented in Fig. 21, indicates that as the ellipse becomes thinner and closer to a crack shape, the stress in  $\theta = 0^\circ$  tends to the nominal applied load, while it is virtually constant in  $\theta = 90^\circ$ . Clearly, the independence of  $r_a/r_b$  on compressive strength curves indicates that the

matrix is failing under tension in  $\theta = 90^\circ$ , as presented in Fig. 22. However, once again the LaRC05 indicates fiber failure, while the Puck model indicates the matrix failure.

#### 4 Three-dimensional effects

Góes et al. [2] presented results showing the influence of non-negligible 3D effects in the stress concentration for notched isotropic materials that are usually neglected when the notches are treated as 2D geometries. Based on those results, it can be expected that for anisotropic materials the thickness also influences the stress distribution and failure predictions. Nevertheless, most numerical simulations and analytical approaches use 2D geometries and plane stress hypothesis for model composite plates. In this section, an analytical study of the plane strain assumption is introduced, since this hypothesis is a simplified

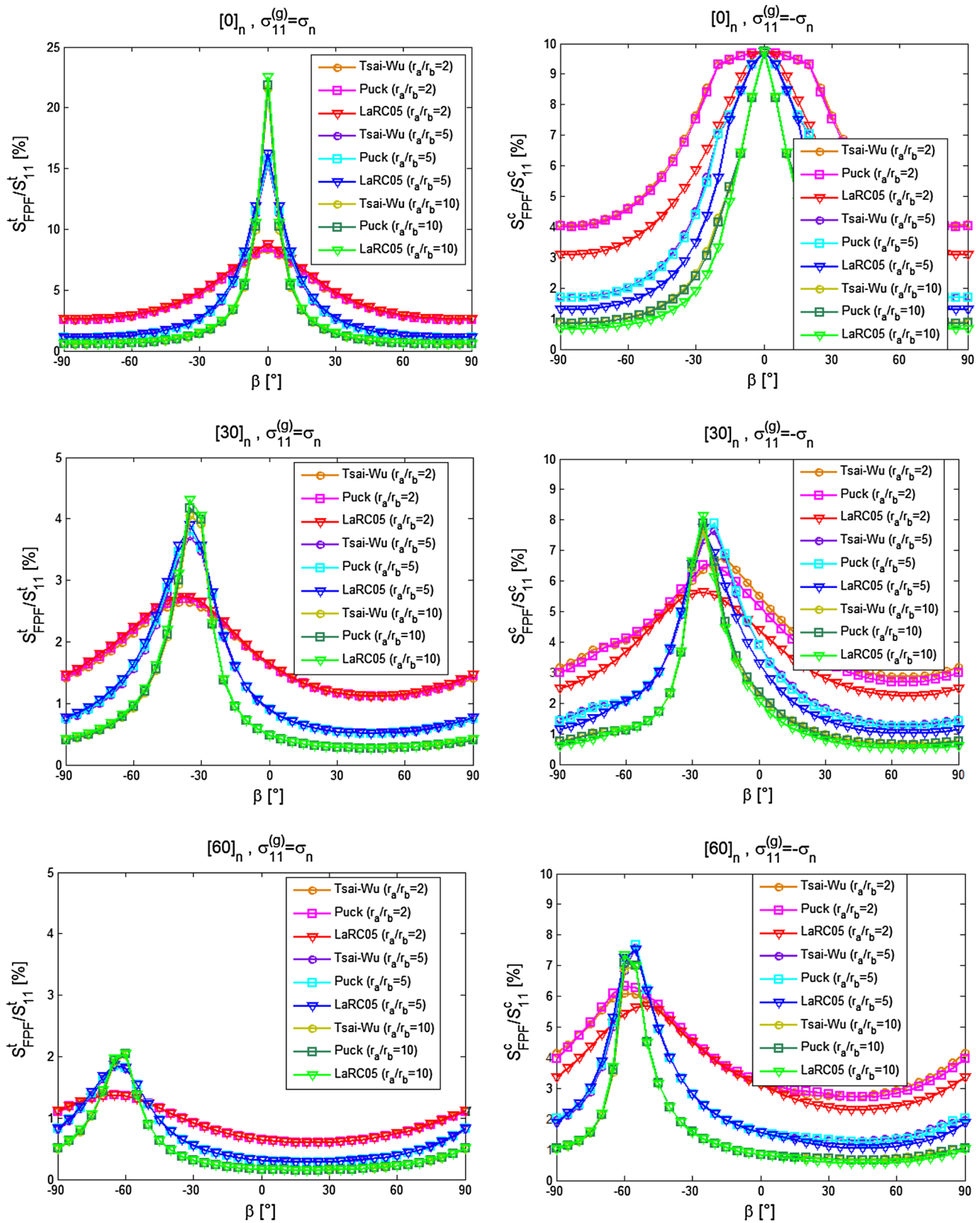


Fig. 19 Prediction of tension and compression FPF strength of large plates with elliptical holes

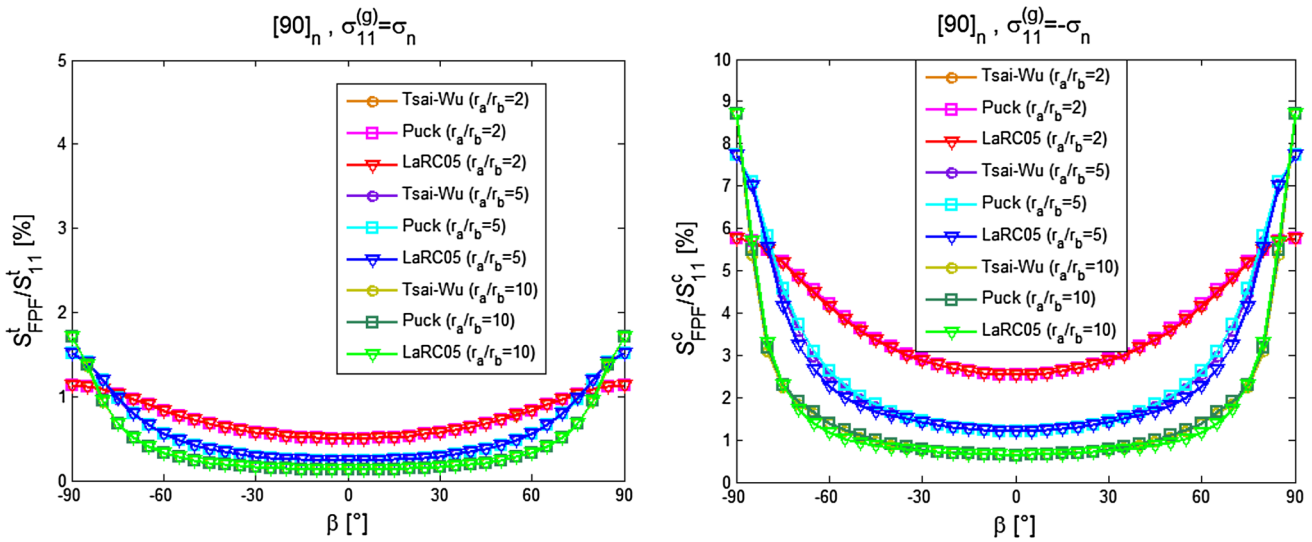


Fig. 19 (continued)

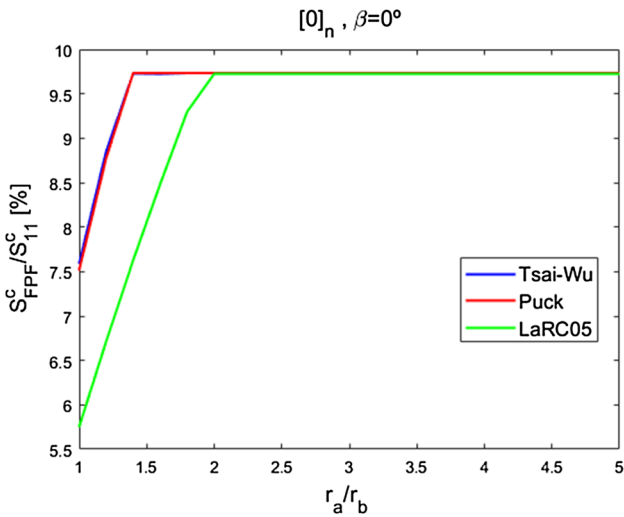


Fig. 20 Variation of compression FPF strength of large plates with central elliptical holes parallel to the fibers direction according to the ellipse aspect or axes ratio  $r_a/r_b$

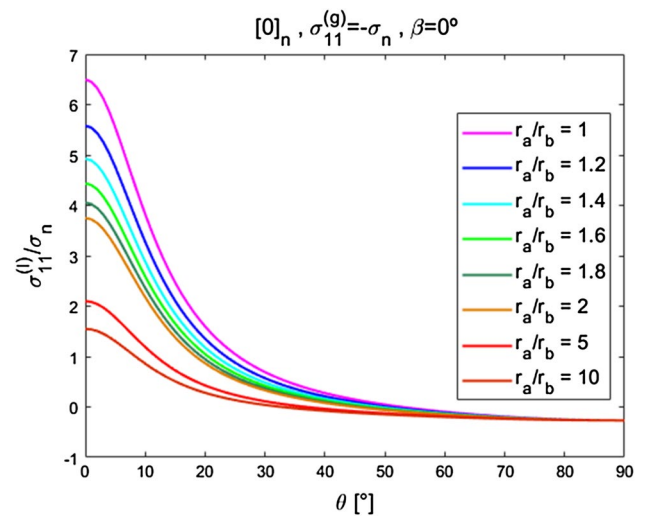


Fig. 21 Stress concentration for large plates with elliptical holes parallel to the fibers

bound for real plates. To evaluate the thickness effects, the transversal constraint factor defined in Eq. (40) can be useful:

$$T_c = \frac{\sigma_{33}^{(l)}}{\sigma_{11}^{(l)} + \sigma_{22}^{(l)}} \quad (40)$$

Notice that  $T_c$  is defined according to the local coordinates. The material constitutive relation in the local coordinate system is given by

$$\epsilon_{ij}^{(l)} = c_{ijkm}^{(l)} \sigma_{km}^{(l)} \quad (41)$$

where  $c_{ijkm}^{(l)}$  is the compliance tensor in local coordinates. The compliance tensor components for a transversally isotropic material can be defined in simplified matrix form as [2]

$$c = \begin{bmatrix} \frac{1}{E_1} & -\frac{\nu_{12}}{E_1} & -\frac{\nu_{13}}{E_1} & 0 & 0 & 0 \\ -\frac{\nu_{21}}{E_2} & \frac{1}{E_2} & -\frac{\nu_{23}}{E_2} & 0 & 0 & 0 \\ -\frac{\nu_{31}}{E_3} & -\frac{\nu_{32}}{E_3} & \frac{1}{E_3} & 0 & 0 & 0 \\ 0 & 0 & 0 & \frac{1}{G_{23}} & 0 & 0 \\ 0 & 0 & 0 & 0 & \frac{1}{G_{13}} & 0 \\ 0 & 0 & 0 & 0 & 0 & \frac{1}{G_{12}} \end{bmatrix} \quad (42)$$

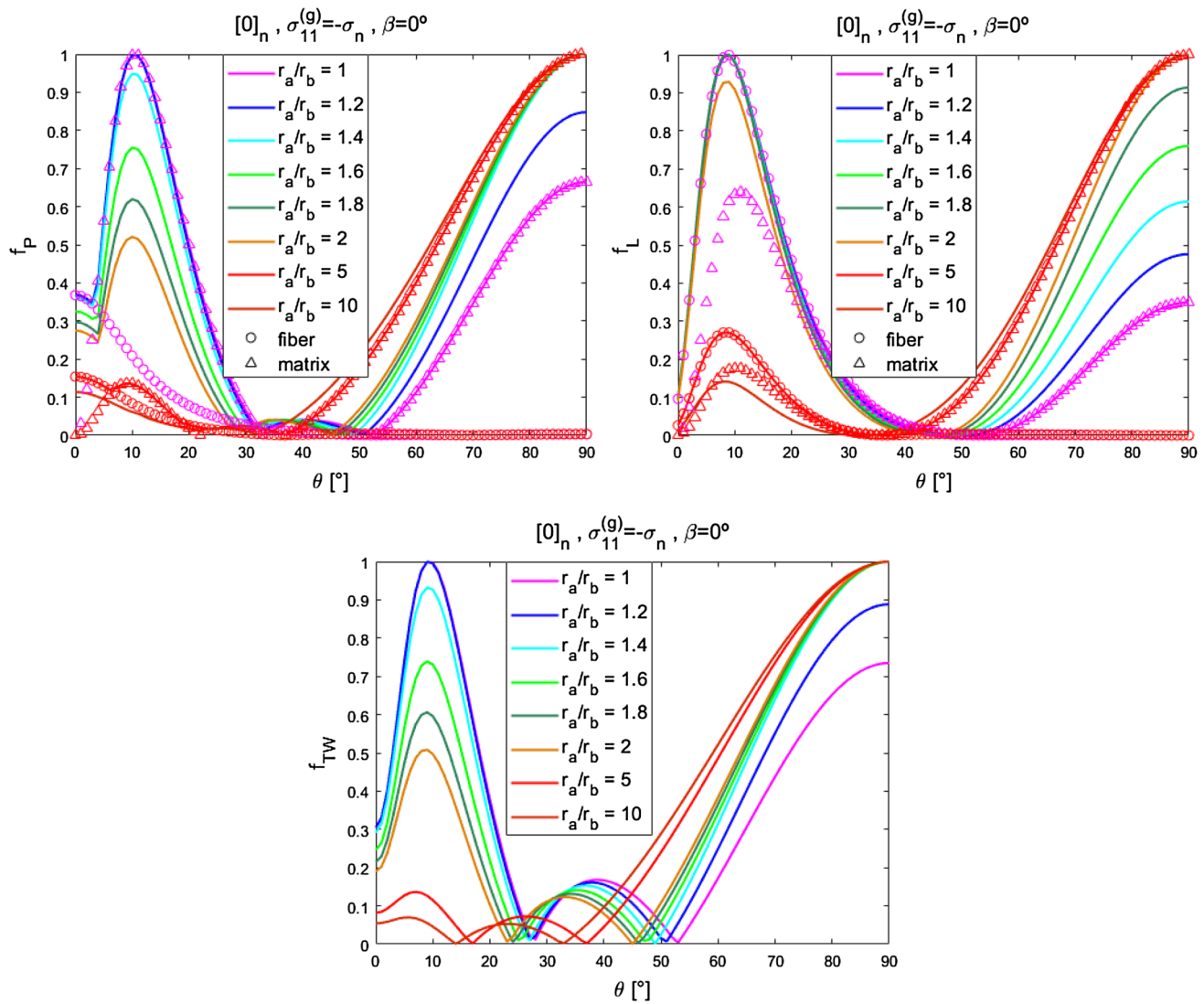


**Fig. 22** Variation of the failure functions for compressed large plates with central elliptical holes parallel to the fibers direction

To compute the compliance components in local coordinates, the following transformation must be used

$$c_{ijkl}^{(l)} = \lambda_{im} \lambda_{jn} \lambda_{ko} \lambda_{lp} c_{mnop} \tag{43}$$

For plane stress,  $\sigma_{33}^{(l)} = 0$  and consequently  $T_c = 0$ . For plane strain, along the elliptical hole border, remembering that the  $x_2^{(l)}$  is the surface free direction perpendicular to the hole (see Fig. 1), the transversal strain obeys

$$\epsilon_{33}^{(l)} = c_{3311}^{(l)} \sigma_{11}^{(l)} + c_{3333}^{(l)} \sigma_{33}^{(l)} = 0 \tag{44}$$

Thus, the transversal constraint factor is

$$T_c = \frac{\sigma_{33}^{(l)}}{\sigma_{11}^{(l)}} = -\frac{c_{3311}^{(l)}}{c_{3333}^{(l)}} \tag{45}$$

For plane stress,  $\sigma_{33}^{(l)} = 0$  and consequently  $T_c = 0$ . For plane strain, along the elliptical hole border, remembering that the  $x_2^{(l)}$  is the surface free direction perpendicular to the hole (see Fig. 1), the transversal strain obeys

$$\epsilon_{33}^{(l)} = c_{3311}^{(l)} \sigma_{11}^{(l)} + c_{3333}^{(l)} \sigma_{33}^{(l)} = 0 \tag{44}$$

Thus, the transversal constraint factor is

$$T_c = \frac{\sigma_{33}^{(l)}}{\sigma_{11}^{(l)}} = -\frac{c_{3311}^{(l)}}{c_{3333}^{(l)}} \tag{45}$$

Notice that  $c_{3313}^{(l)} = 0$  and  $\sigma_{33}^{(l)} = \sigma_{33}$  along the elliptical hole border, because its axis rotation is on the plane  $x_1 - x_2$ . If the material is isotropic,  $c_{3311}^{(l)} = c_{3311}$  and  $c_{3333}^{(l)} = c_{3333}$ , resulting

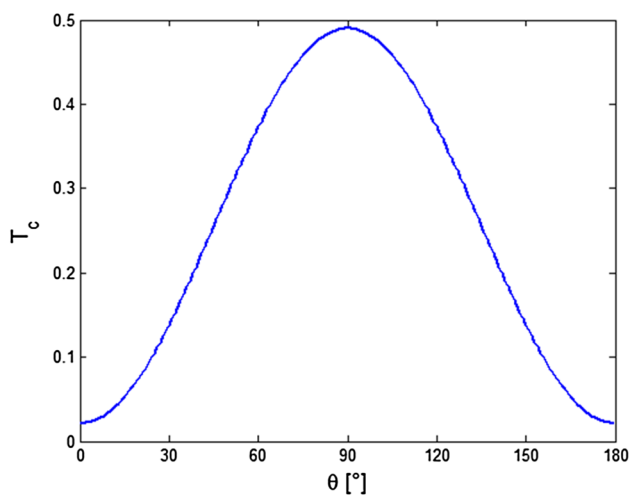


**Fig. 23** Constraint factor variation along the elliptical hole border for plane strain in a AS carbon/epoxy composite

in  $T_c = \nu$ , as observed by Góes et al. [2]. The constraint factor variation along the hole border for the laminate  $[\alpha]_n$  with the material properties from Table 1 is presented in Fig. 23. Since the constraint factor is not constant, the stress components in material coordinates are not multiplied by the same value along the border, resulting in a completely different stress distribution. Notice that Fig. 23 is independent of the fiber-to-load angle, the load, and the hole geometry, it depends just on the material properties.

Plane strain and plane stress assumptions are limit cases for thick and thin plates that can be used to estimate thickness effects. For plane strain, some quantities defined on the Stroh formalism must be modified. The details are omitted in this text, but can be found in [4, 6]. For a large plate with a circular hole under a uniaxial applied load, as considered previously for plane stress, the components of stress concentration variation in material coordinate are presented in

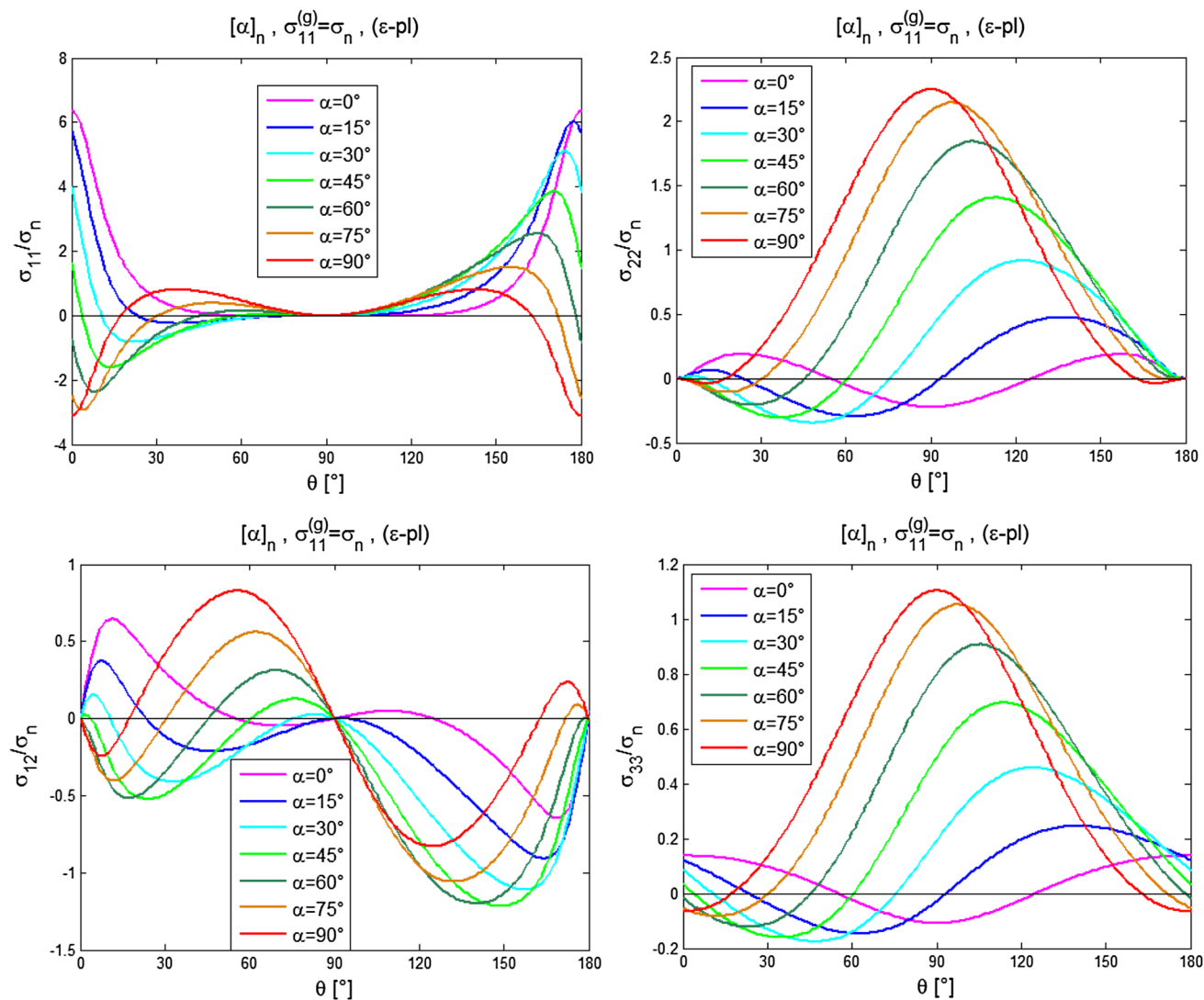


**Fig. 24** Stress concentration for a structure under plane strain and uniaxial applied load

Fig. 24. Notice that now there is one more stress component and that this additional component, namely  $\sigma_{33}$ , can be even larger than the nominal applied stress depending on the fibers-to-load angle, indicating that the failure predictions are highly sensible to the assumptions adopted.

For plane strain, the strengths were obtained following the same procedure used for plane stress and are presented in Fig. 25. Since the aim of this study is to evaluate possible stress concentration issues, the strengths estimated for plane stress are also plotted together to permit a direct comparison. For tensile loads, the failure tendencies remain similar, but for compression the results are very different, both in curve shapes and magnitudes. The largest variation is for the LaRC05 criterion, because the multi-axial stress state has a non-negligible influence in fiber stability [48, 51].

Some load conditions were selected for a more detailed analysis presented in Fig. 26. First, for  $\sigma_{11}^{(g)} = 70$  MPa and  $\alpha = 0^\circ$ , just Tsai–Wu’s model predicts failure, due to the direct sum of one more stress component of the polynomial function, while for the other models, the critical plane search is not so sensitive to one more normal stress component. This conclusion can be realized for general tensile strengths: just Tsai–Wu indicates the tendency for strength decrease. For the compressive loads, three different results are shown: for  $\sigma_{11}^{(g)} = -70$  MPa and  $\alpha = 15^\circ$ , just LaRC05 indicates failure on the fibers; for  $\sigma_{11}^{(g)} = -70$  MPa and  $\alpha = 45^\circ$ , Tsai–Wu’s is the only one that indicates a safe condition, and for  $\sigma_{11}^{(g)} = -60$  MPa and  $\alpha = 75^\circ$ , only the LaRC05 does not predict failure. No definitive conclusion may be obtained from these results, due to the wide range of different predictions, but the results from the WWFE-II [30] show that for 3D stress states, the critical plane search becomes even more important and the physically

based models are more recommended than the polynomial fitted ones.

The Tsai–Wu criterion predicts a very peculiar behavior for the FPF compressive strength. To enlighten why the curve has so many abrupt variations, mainly because this failure function is not able to different matrix and fiber failure, the variation of the Tsai–Wu failure function according to the  $\theta$  for different values of  $\alpha$  is presented in Fig. 27. With this one more stress component on the polynomial function, the failure location becomes highly sensitive to the fiber orientation.

Góes et al. [2] obtained a difference on the strength prediction between plane stress and plane strain limit cases smaller than 10% using Tresca and von Mises criteria for isotropic materials. For these unidirectional laminates, the ratios between the strengths for plane strain and plane stress are represented in Fig. 28. To assume a plane stress condition can be a conservative hypothesis or not, depending on the criteria applied, the fiber-to-load angle, and the applied load. However, some major issues must be highlighted about these assumptions: Tsai–Wu and Puck predicted strengths differences larger than 20%, which is already an alarming result; LaRC05 predictions indicate a difference larger than 50%, clearly evidencing the gap between 2D assumptions and the possible thickness effects, indicating once more the need for reliable experimental data to validate the anisotropic damage models. Therefore, numerical simulations with 3D geometries are recommended before using simplified 2D assumptions for design if the slenderness of the laminate is not assured.

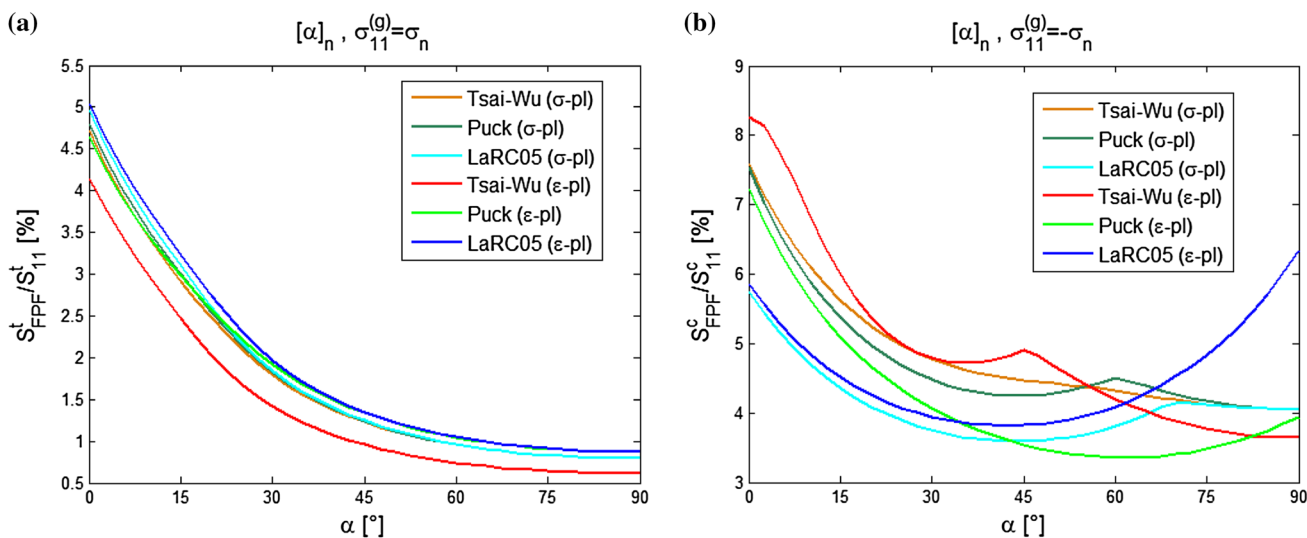


Fig. 25 Prediction of maximum applied tension **a** and compression **b** load for initial damage in a structure under plane strain

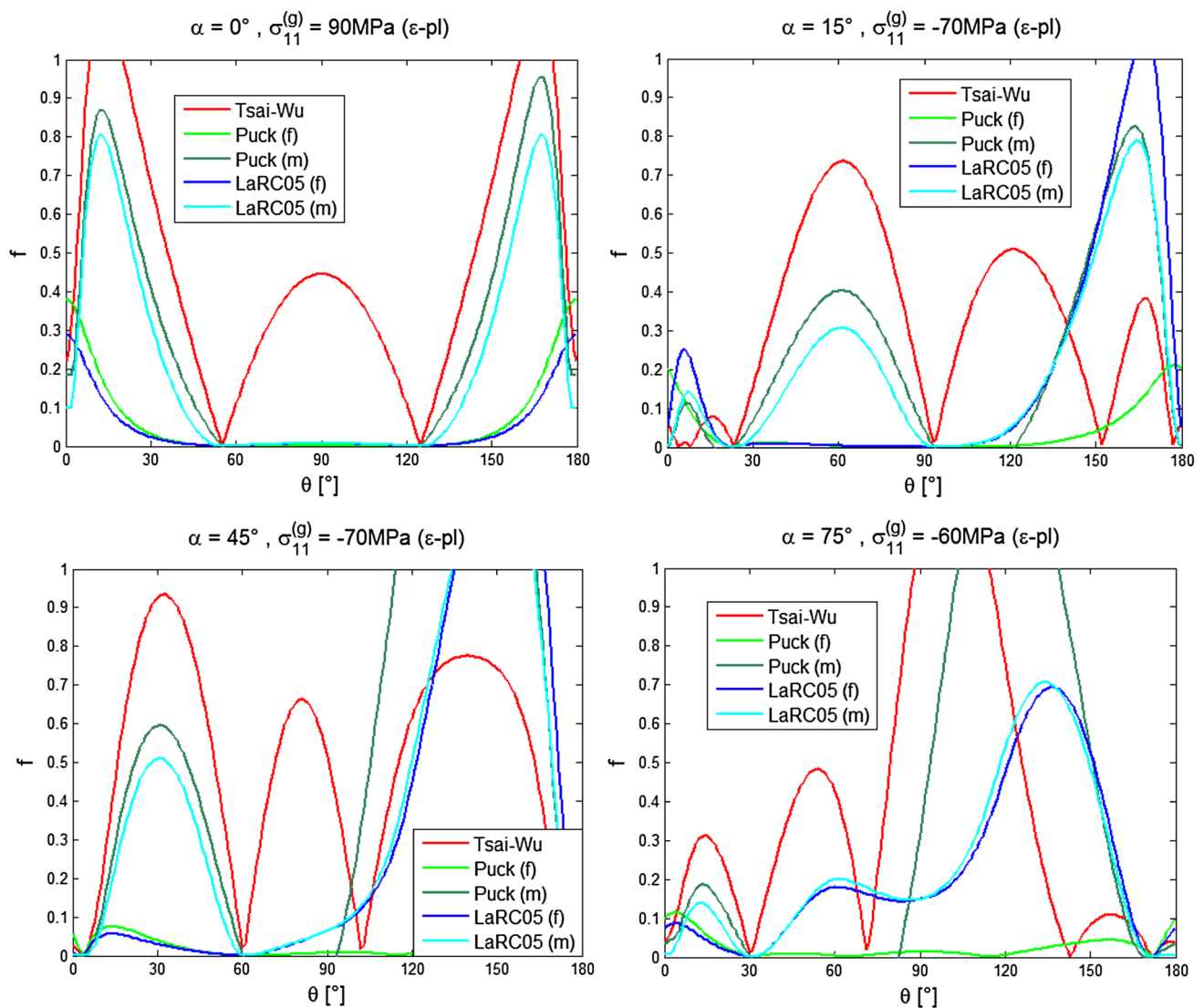


Fig. 26 Selected cases for uniaxial applied stress considering the plane strain

## 5 Conclusions

This paper first reviews some theoretical approaches for predicting the strength of anisotropic materials, in particular, of laminate composites. Then, it applies three failure theories, chosen considering the WWFE results and recommendations, to study stress concentration effects on single-layer laminated plates: Tsai–Wu, Puck, and LaRC05.

The failure models are compared considering different load conditions, fibers orientation, and circular and elliptical hole geometries. Tsai–Wu has a simple form and is represented by just one equation, resulting in an easier implementation, saving computational cost. On the other hand, Puck and LaRC05 have different models for fiber and matrix failure under compression and tension, resulting in three or four different equations, thus requiring more time to

compute their predictions. Nevertheless, this effort is justified by the gain it allows in the physical understanding of the failure process. Especially for fibers under compression, the LaRC05 model leads to very different predictions from the other models, and for some conditions, it predicts failure considerably earlier than Puck’s and Tsai–Wu criteria, due to the shear influence on the laminate failure for longitudinal compression. On the other hand, Puck’s criterion is also able to distinguish different failure mechanism using the critical plane concept, but has the advantage to have explicit expressions for matrix failure only for plane stress conditions. This way, the computational critical plane search is not necessary, which is a major advantage for numerical implementations.

Large plates made by single-layered unidirectional laminates with circular holes had a FPF strength decrease estimation of more than 95%, 90% and 20% for uniaxial tension,

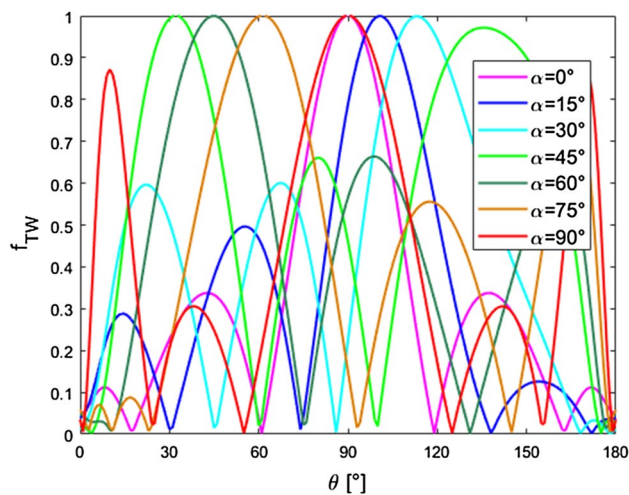


**Fig. 27** Tsai–Wu failure function for different fibers orientation

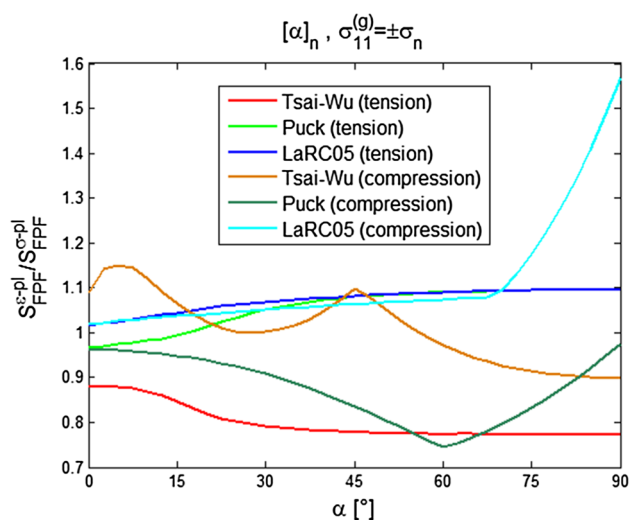


**Fig. 28** Difference of the strengths for plane stress and plane strain hypotheses

compression, and pure shear loads, respectively. These results become even more pronounced, depending on the fiber orientation.

For elliptical holes, some results are presented to enhance the influence of the hole inclination and laminate angle. It is observed that the inclination that induces maximum stress concentration for uniaxial loads is somewhere between the direction perpendicular to the applied load and the direction perpendicular to the fiber. However, as clearly demonstrated for circular holes where the laminate angle is the single variable that affects it, the maximum stress concentration does not represent the critical point.

Finally, the plane strain hypothesis is analyzed to study the thickness influence on the laminate failure. There are

large differences between plane stress and plane strain predictions: larger than 20% according to Tsai–Wu and Puck criteria and larger than 50% according to LaRC05 criterion, indicating that it may be unsafe to consider plane stress as a simplifying assumption.

In summary, the major contributions of the present study are:

1. For unidirectional loads on single-layer laminates with a circular hole, the stress concentration may be as large as 7 or more than twice higher than the well-known result for isotropic materials;
2. Due to this severe stress concentration effect around the notches, matrix failure is predicted for most cases, and the notched strength of single-layer laminates can be smaller than 10% of their unnotched strength;
3. Pure shear and biaxial tension/compression cannot be directly compared as equivalent conditions in notched single-layer laminates;
4. The difference of strength predictions assuming plane stress and plane strain limit hypotheses may be higher than 50%, so thickness effects can be very important in single-layer laminates; and
5. For tension loads, all the studied failure criteria indicate similar predictions, but for compression, the LaRC05 model indicates a considerable strength reduction when compared to the other models, due to the fibers instability for combined longitudinal compression and shear.

## References

1. Savin GN (1970) Stress distribution around holes. NASA Technical Translation, Washington, DC
2. Góes RCO, Castro JTP, Meggiolaro MA (2014) 3D thickness effects around notch and crack tips. *Int J Fatigue* 62:159–170
3. Lekhniskii SG (1981) Theory of elasticity of an anisotropic body. Mir Publishers, Moscow
4. Ting TCT (1996) Anisotropic elasticity: theory and applications. Oxford University Press, Oxford
5. Lekhniskii SG (1987) Anisotropic plates, 3rd edn. Gordon and Breach Science Publishers, New York
6. Hwu C (2009) Anisotropic elastic plates. Springer, Berlin
7. Tan SC (1987) Laminated composites containing an elliptical opening. I. Approximate stress analyses and fracture models. *J Compos Mater* 21:925–948
8. Tan SC (1988) Finite-width correction factors for anisotropic plate containing a central opening. *J Compos Mater* 22:1080–1097
9. Kaman MO (2011) Effect of fiber orientation on fracture toughness of laminated composite plates  $[0/\theta]_s$ . *Eng Fract Mech* 78:2521–2534
10. Zappalorto M, Carraro PA (2015) An engineering formula for the stress concentration factor of orthotropic composite plates. *Compos Part B Eng* 68:51–58
11. Sevenois RDB, Koussios S (2014) Analytic methods for stress analysis of two-dimensional flat anisotropic plates with notches: an overview. *Appl Mech Rev* 66:060802-1–060810-1

12. Whitney JM, Nuismer RJ (1974) Stress fracture criteria for laminated composites containing stress concentration. *J Compos Mater* 8:253–265
13. Iarve EV, Mollenhauer D, Kim R (2005) Theoretical and experimental investigation of stress redistribution in open hole composite laminates due to damage accumulation. *Compos Part A Appl S* 36:163–171
14. Mollenhauer D, Iarve EV, Kim R, Langley B (2006) Examination of ply cracking in composite laminates with open holes: a moiré interferometric and numerical study. *Compos Part A Appl S* 37:282–294
15. O'Higgins RM, McCarthy MA, McCarthy CT (2008) Comparison of open hole tension characteristics of high strength glass and carbon fibre-reinforced composite. *Compos Sci Technol* 68:2770–2778
16. Lee J, Soutis C (2008) Measuring the notched compressive strength of composite laminates: Specimen size effects. *Compos Sci Technol* 68:2359–2366
17. Huang Y, Ha SK, Koyanagi J, Melo JDD, Kumazawa H, Susuki I (2010) Effects of an open hole on the biaxial strengths of composite laminates. *J Compos Mater* 44:2429–2445
18. Kureemun U, Ridha M, Tay TE (2015) Biaxial tensile-compressive loading of unnotched and open-hole carbon epoxy crossply laminates. *J Compos Mater* 49:2817–2837
19. Shah PD, Melo JDD, Cimini CA Jr, Ridha M (2010) Evaluation of notched strength of composite laminates for structural design. *J Compos Mater* 44:2381–2392
20. Chen BY, Tay TE, Baiz PM, Pinho ST (2013) Numerical analysis of size effects on open-hole tensile composite laminates. *Compos Part A Appl S* 47:52–62
21. Su ZC, Tay TE, Ridha M, Chen BY (2015) Progressive damage modeling of open-hole composite laminates under compression. *Compos Struct* 122:507–517
22. Sadeghi G, Hosseini-Toudeshky H, Mohammadi B (2014) An investigation of matrix cracking damage evolution in composite laminates – Development of an advanced numerical tool. *Compos Struct* 108:937–950
23. Moure MM, Otero F, García-Castillo SK, Sánchez-Sáez S, Barbero E, Barbero EJ (2015) Damage evolution in open-hole laminated composite plates subjected to in-plane loads. *Compos Struct* 133:1048–1057
24. Andrianov IV, Awrejcewicz J, Danishevskyy VV (2018) Asymptotical mechanics of composites—modelling composites without FEM. Springer, Berlin
25. Vignoli LL, Savi MA (2018) Multiscale failure analysis of cylindrical composite pressure vessel: a parametric study. *Latin Am J Solids Struct* 15:1–20
26. Zappalorto M, Carraro PA (2015) Stress distributions for blunt cracks and radiused slits in anisotropic plates under in-plane loadings. *Int J Solids Struct* 56–57:136–141
27. Zappalorto M (2017) On the stress state in rectilinear anisotropic thick plates with blunt cracks. *Fatigue Fract Eng Mater Struct* 40:103–119
28. Bonora N, Costanzi M, Marchetti M (1993) On closed form solution for the elastic stress field around holes in orthotropic composite plates under in-plane stress conditions. *Compos Struct* 25:139–156
29. Bonora N, Costanzi M, Marchetti M (1994) A computational procedure to calculate stress-strain field around simple shape holes in composite laminates. *Compos Struct* 53:1167–1179
30. Hinton MJ, Kaddour AS, Soden PD (2004) Failure criteria in fibre reinforced polymer composites: the world-wide failure exercise. Elsevier, Amsterdam
31. Soden PD, Kaddour AS, Hinton MJ (2004) Recommendations for designers and researchers resulting from the world-wide failure exercise. *Compos Sci Technol* 64:589–604
32. Kaddour AS, Hinton MJ (2013) Maturity of 3D failure criteria for fibre reinforced composites: Comparison between theories and experiments: Part B of WWFE-II. *J Compos Mater* 47:925–966
33. Sokolnikoff IS (1956) Mathematical theory of elasticity, 2nd edn. McGraw-Hill Book Company, New York
34. Barnett DM, Lothe J (1973) Synthesis of the sextic and the integral formalism for dislocation, green's function and surface waves in anisotropic elastic solids. *Phys Norv* 7:13–19
35. Barbero EJ (2018) Introduction to composite materials design, 3rd edn. CRC Press, Boca Raton
36. Jones RM (1998) Mechanics of composite materials, 2nd edn. Taylor & Francis Editions, Boca Raton
37. Vasiliev VV, Morozov EV (2001) Mechanics and analysis of composite materials. Elsevier, Amsterdam
38. Kant T, Swaminathan K (2000) Estimation of transverse/interlaminar stresses in laminated composites - a selective review and survey of current developments. *Compos Struct* 49:65–75
39. Cuntze RG, Freund A (2004) The predictive capability of failure mode concept-based strength criteria for multidirectional laminates. *Compos Sci Technol* 64:343–377
40. Tsai SW, Melo JDD (2014) An invariant-based theory of composites. *Compos Sci Technol* 100:237–243
41. Vignoli LL, Savi MA, Pacheco PMCL, Kalamkarov AL (2019) Comparative analysis of micromechanical models for the elastic composite laminae. *Compos Part B* 174:106961
42. Tsai SW, Wu EM (1971) A general theory of strength for anisotropic materials. *J Compos Mater* 5:58–80
43. Liu KS, Tsai SW (1998) A progressive quadratic failure criterion for a laminate. *Compos Sci Technol* 58:1023–1032
44. Puck A, Schürmann H (1998) Failure analysis of FRP laminates by means of physically based phenomenological models. *Compos Sci Technol* 58:1045–1067
45. Deuschle HM, Puck A (2013) Application of the Puck failure theory for fibre-reinforced composites under three-dimensional stress: Comparison with experimental results. *J Compos Mater* 47:827–846
46. VDI Guideline 2204 (2006) Part 3: Development of Fibre-Reinforced-Plastics components, Analysis, Issue German/English. Beuth-Verlag, Berlin
47. Knops M (2008) Analysis of failure in fiber polymer laminates—the theory of Alfred Puck. Springer, Berlin
48. Pinho ST, Darvizeh R, Robinson P, Schuecker C, Camanho PP (2012) Material and structural response of polymer-matrix fibre-reinforced composites. *J Compos Mater* 46:2313–2341
49. Pinho ST, Iannucci L, Robinson P (2006) Physically-based failure models and criteria for laminated fibre-reinforced composites with emphasis on fibre kinking: Part I: Development. *Compos Part A Appl S* 37:63–73
50. Pinho ST, Dávila CG, Camanho PP, Iannucci L, Robinson P (2005) Failure models and criteria for FRP under in-plane or three-dimensional stress states including shear non-linearity. NASA/TM-2005-213530
51. Pimenta S, Gutkin R, Pinho ST, Robinson P (2009) A micromechanical model for kink-band formation: Part I - Experimental study and numerical modelling. *Compos Sci Technol* 69:948–955
52. Kaddour AS, Hinton MJ (2012) Input data for test cases used in benchmarking triaxial failure theories of composites. *J Compos Mater* 46:2295–2312
53. Kalamkarov AL, Kolpakov AG (1997) Analysis, design and optimization of composite structures, 2nd edn. Wiley, New York
54. Inglis CE (1913) Stresses in a plate due to the presence of cracks and sharp corners. *Trans Inst Naval Archit* 55:219–241
55. Meggiolaro MA, Miranda ACO, Castro JTP (2007) Short crack threshold estimates to predict notch sensitivity factors in fatigue. *Int J Fatigue* 29:2022–2031

56. Castro JTP, Meggiolaro MA, Miranda ACO, Wu H, Imad A, Nouredine B (2012) Prediction of fatigue crack initiation lives at elongated notch roots using short crack concepts. *Int J Fatigue* 42:172–182
57. Castro JTP, Landim RV, Meggiolaro MA (2015) Defect tolerance under environmentally-assisted cracking conditions. *Corros Rev* 33:417–432
58. Castro JTP, Meggiolaro MA (2016) *Fatigue design techniques. I High-Cycle Fatigue*, CreateSpace
59. Hwu C, Ting TCT (1989) Two-dimensional problems of the anisotropic elastic solid with an elliptic inclusion. *Q J Mech Appl Math* 42:553–572

**Publisher's Note** Springer Nature remains neutral with regard to jurisdictional claims in published maps and institutional affiliations.